

Strong $U_A(1)$ breaking in radiative η decays

M. Takizawa¹

*Institute for Nuclear Study, University of Tokyo,
Tanashi, Tokyo 188, Japan*

Y. Nemoto² and M. Oka³

*Department of Physics, Tokyo Institute of Technology,
Meguro, Tokyo 152, Japan*

Abstract

We study the $\eta \rightarrow \gamma\gamma$, $\eta \rightarrow \gamma\mu^-\mu^+$ and $\eta \rightarrow \pi^0\gamma\gamma$ decays using an extended three-flavor Nambu-Jona-Lasinio model that includes the 't Hooft instanton induced interaction. We find that the η -meson mass, the $\eta \rightarrow \gamma\gamma$, $\eta \rightarrow \gamma\mu^-\mu^+$ and $\eta \rightarrow \pi^0\gamma\gamma$ decay widths are in good agreement with the experimental values when the $U_A(1)$ breaking is strong and the flavor $SU(3)$ singlet-octet mixing angle θ is about zero. The calculated $\eta\gamma\gamma^*$ transition form factor has somewhat weaker dependence on the squared four-momentum of the virtual photon. The effects of the $U_A(1)$ anomaly on the scalar quark contents in the nucleon, the $\Sigma_{\pi N}$ and Σ_{KN} terms and the baryon number one and two systems are also studied.

1 Introduction

It is well known that the QCD action has an approximate $U_L(3) \times U_R(3)$ chiral symmetry and its sub-symmetry, $U_A(1)$ symmetry, is explicitly broken by the anomaly. The $U_A(1)$ symmetry breaking is manifested in the heavy mass of the η' meson. The physics of the η and η' mesons have been extensively studied in the $1/N_C$ expansion approach [1]. In the $N_C \rightarrow \infty$ limit, the $U_A(1)$ anomaly is turned off and then the η meson becomes degenerate with the pion and the η' meson becomes a pure $\bar{s}s$ state with $m_{\eta'}^2(N_C \rightarrow \infty) \simeq 2m_K^2 - m_\pi^2 \simeq (687 \text{ MeV})^2$ [2]. So

¹E-mail address: takizawa@ins.u-tokyo.ac.jp

²E-mail address: nemoto@th.phys.titech.ac.jp

³E-mail address: oka@th.phys.titech.ac.jp

the $U_A(1)$ anomaly pushes up m_η by about 400MeV and $m_{\eta'}$ by about 300MeV. It means that not only the η' meson but also the η meson is largely affected by the $U_A(1)$ anomaly.

In order to understand the role of the $U_A(1)$ anomaly in the low-energy QCD, it may be important to study the η -meson decays as well as its mass and decay constant. Among the η -meson decays, $\eta \rightarrow \gamma\gamma$, $\eta \rightarrow \gamma l^- l^+$ (l denotes e and/or μ) and $\eta \rightarrow \pi^0\gamma\gamma$ decays are interesting. They have no final state interactions and involve only neutral mesons so that the electromagnetic transitions are induced only by the internal (quark) structure of the mesons.

The $\eta \rightarrow \gamma\gamma$ decay is related to the Adler-Bell-Jackiw (ABJ) triangle anomaly [3] through the partial conservation of axialvector current (PCAC) hypothesis. One of the useful and widely used frameworks for studying the phenomena related to the axial-vector anomaly and the spontaneous chiral symmetry breaking is the chiral effective meson lagrangian given by Wess and Zumino [4] and developed by Witten [5]. The $\eta, \eta' \rightarrow \gamma\gamma$ decays have been studied using the Wess-Zumino-Witten (WZW) lagrangian with the corrections at one-loop order in the chiral perturbation and it has been shown that the two-photon decay widths can be explained with the η - η' mixing angle $\theta \simeq -20^\circ$ [6]. From the chiral perturbation theory (ChPT) [7] point of view, the WZW term is derived in the chiral limit and is of order p^4 . As discussed in [8], to reliably calculate $SU(3)$ breaking effects of the $\eta, \eta' \rightarrow 2\gamma$ decays, the low-energy expansion to order p^6 has to be carried out. However in [6] full analysis of order p^6 has not been performed. Furthermore, because of the $U_A(1)$ anomaly, the singlet channel decay amplitude $\eta_0 \rightarrow \gamma\gamma$ derived using PCAC + ABJ anomaly should be modified so as to become renormalisation group invariant [9].

The $\eta \rightarrow \gamma l^- l^+$ decay is closely related to the $\eta \rightarrow \gamma\gamma$ decay since it is considered as $\eta \rightarrow \gamma\gamma^* \rightarrow \gamma l^+ l^-$. By observing the muon pair invariant mass square spectrum of the $\eta \rightarrow \gamma l^- l^+$ decay, one is able to obtain the transition form factor for the $\eta\gamma\gamma^*$ vertex. It gives us the information of the size of the η -meson. In [10] the transition form factors for the $\pi^0\gamma\gamma^*$, $\eta\gamma\gamma^*$ and $\eta'\gamma\gamma^*$ vertices have been studied in the vector meson dominance model, the constituent quark loop model, the QCD-inspired interpolation model by Brodsky-Lepage and the ChPT. However none of the models have taken into account the effects of the $U_A(1)$ anomaly explicitly.

Unlike the $\eta \rightarrow \gamma\gamma$ decay, there is no low-energy theorem for the $\eta \rightarrow \pi^0\gamma\gamma$ decay and therefore it is not trivial. In ChPT [11–13], there is no lowest order $O(p^2)$ contribution to the $\eta \rightarrow \pi^0\gamma\gamma$ process because the involved mesons are neutral. Likewise the next order $O(p^4)$ tree diagrams do not exist. Thus the $O(p^4)$ one-loop diagrams give the leading term in this process, but the contribution is two orders of magnitude smaller than the experimental value. This is because the pion loop violates the G-parity invariance and the kaon loop is also suppressed by the large kaon mass. The $O(p^6)$ contributions are dominant and the result is a factor two smaller than the experimental value. Although these results based on ChPT are not too far from the experimental value, it is noted that the higher order $O(p^6)$ terms in the perturbation expansion are larger than the leading $O(p^4)$ terms and the results contain ambiguous parameters that cannot be determined well from other processes.

The purpose of this paper is to study the $\eta \rightarrow \gamma\gamma$, $\eta \rightarrow \gamma l^- l^+$ and $\eta \rightarrow \pi^0\gamma\gamma$ decays in the framework of a chiral quark model so that the quark structure of the η meson is explicitly taken into account. In such a model the explicit chiral symmetry breaking by the current quark masses can be included in a nonperturbative way. The effects of the $U_A(1)$ anomaly can also be represented by the coupling of light quarks to the instanton as was pointed out by 't Hooft [14]. We here take the three-flavor Nambu-Jona-Lasinio (NJL) model as the chiral quark model. The model involves the $U_L(3) \times U_R(3)$ symmetric four-quark interaction and the six-quark flavor-determinant interaction [14, 15] incorporating effects of the $U_A(1)$ anomaly. It is widely used in recent years to study such topics as the quark condensates in vacuum, the spectrum of low-lying mesons, the flavor-mixing properties of the low-energy hadrons, etc. [16–21]. In this approach the explicit chiral symmetry breaking and the $U_A(1)$ anomaly on the $\eta \rightarrow \gamma\gamma$, $\eta \rightarrow \gamma l^- l^+$ and $\eta \rightarrow \pi^0\gamma\gamma$ decay amplitudes can be calculated consistently with those on the η -meson mass, η decay constant and mixing angle within the model applicability. Furthermore one is able to study how the η -meson properties change when the strength of the $U_A(1)$ breaking interaction is changed in this approach.

We have studied the $\eta \rightarrow \gamma\gamma$ decay [22] and the $\eta \rightarrow \pi^0\gamma\gamma$ decay [23] in this approach and found that these decay widths are reproduced when the $U_A(1)$ breaking interaction is much stronger than the previous studies in the three-flavor NJL model [16–21]. The $U_A(1)$ breaking six-quark flavor-determinant interaction

induced by the instanton [14] gives rise to flavor mixing not only in the pseudoscalar channel but also in the scalar channel. It is further argued that the instanton can play an important role in description of spin-spin forces, particularly for light baryons [24–26]. Since the $U_A(1)$ breaking interaction is found to be rather strong, it is important to reexamine the effects of the $U_A(1)$ breaking interaction on the scalar quark contents in the nucleon, the $\Sigma_{\pi N}$ and Σ_{KN} terms and the baryon number one and two systems.

The paper is organized as follows. In sect. 2 we explain methods for calculating the η -meson mass, mixing angle and decay constant in the three-flavor NJL model. We describe the calculations of the $\eta \rightarrow \gamma\gamma$, $\eta \rightarrow \gamma\mu^-\mu^+$ and $\eta \rightarrow \pi^0\gamma\gamma$ decay amplitudes in sect. 3. The numerical results of the η -meson decays are presented in sect. 4. We study the $\bar{u}u$, $\bar{d}d$ and $\bar{s}s$ contents in the nucleon and the $\Sigma_{\pi N}$ and Σ_{KN} terms in sect. 5. Sect. 6 is devoted to the study of the effects of the $U_A(1)$ breaking interaction on the baryon number one and two systems. Finally, summary and concluding remarks are given in sect. 7.

2 η -meson in the three-flavor NJL model

We work with the following NJL model lagrangian density:

$$\mathcal{L} = \mathcal{L}_0 + \mathcal{L}_4 + \mathcal{L}_6, \quad (1)$$

$$\mathcal{L}_0 = \bar{\psi} (i\partial_\mu \gamma^\mu - \hat{m}) \psi, \quad (2)$$

$$\mathcal{L}_4 = \frac{G_S}{2} \sum_{a=0}^8 \left[(\bar{\psi} \lambda^a \psi)^2 + (\bar{\psi} \lambda^a i\gamma_5 \psi)^2 \right], \quad (3)$$

$$\mathcal{L}_6 = G_D \left\{ \det [\bar{\psi}_i (1 - \gamma_5) \psi_j] + \det [\bar{\psi}_i (1 + \gamma_5) \psi_j] \right\}. \quad (4)$$

Here the quark field ψ is a column vector in color, flavor and Dirac spaces and $\lambda^a (a = 0 \dots 8)$ is the $U(3)$ generator in flavor space. The free Dirac lagrangian \mathcal{L}_0 incorporates the current quark mass matrix $\hat{m} = \text{diag}(m_u, m_d, m_s)$ which breaks the chiral $U_L(3) \times U_R(3)$ invariance explicitly. \mathcal{L}_4 is a QCD motivated four-fermion interaction, which is chiral $U_L(3) \times U_R(3)$ invariant. The 't Hooft determinant \mathcal{L}_6 represents the $U_A(1)$ anomaly. It is a 3×3 determinant with respect to flavor with $i, j = u, d, s$.

Quark condensates and constituent quark masses are self-consistently deter-

mined by the gap equations

$$\begin{aligned} M_u &= m_u - 2G_S\langle\bar{u}u\rangle - 2G_D\langle\bar{d}d\rangle\langle\bar{s}s\rangle, \\ M_d &= m_d - 2G_S\langle\bar{d}d\rangle - 2G_D\langle\bar{s}s\rangle\langle\bar{u}u\rangle, \\ M_s &= m_s - 2G_S\langle\bar{s}s\rangle - 2G_D\langle\bar{u}u\rangle\langle\bar{d}d\rangle, \end{aligned} \quad (5)$$

with

$$\langle\bar{a}a\rangle = -\text{Tr}^{(c,D)}[iS_F^a(x=0)] = -\int^\Lambda \frac{d^4p}{(2\pi)^4} \text{Tr}^{(c,D)}\left[\frac{i}{p_\mu\gamma^\mu - M_a + i\varepsilon}\right]. \quad (6)$$

Here the covariant cutoff Λ is introduced to regularize the divergent integral and $\text{Tr}^{(c,D)}$ means trace in color and Dirac spaces.

The pseudoscalar channel quark-antiquark scattering amplitude

$$\langle p_3, \bar{p}_4; \text{out} | p_1, \bar{p}_2; \text{in} \rangle = (2\pi)^4 \delta^4(p_3 + p_4 - p_1 - p_2) \mathcal{T}_{q\bar{q}} \quad (7)$$

is then calculated in the ladder approximation. We assume the isospin symmetry too. In the η and η' channel, the explicit expression is

$$\mathcal{T}_{q\bar{q}} = -\begin{pmatrix} \bar{u}(p_3)\lambda^8 i\gamma_5 v(p_4) \\ \bar{u}(p_3)\lambda^0 i\gamma_5 v(p_4) \end{pmatrix}^T \begin{pmatrix} A(q^2) & B(q^2) \\ B(q^2) & C(q^2) \end{pmatrix} \begin{pmatrix} \bar{v}(p_2)\lambda^8 i\gamma_5 u(p_1) \\ \bar{v}(p_2)\lambda^0 i\gamma_5 u(p_1) \end{pmatrix}, \quad (8)$$

with

$$A(q^2) = \frac{2}{\det \mathbf{D}(q^2)} \{2(G_0 G_8 - G_m G_m) I^0(q^2) - G_8\}, \quad (9)$$

$$B(q^2) = \frac{2}{\det \mathbf{D}(q^2)} \{-2(G_0 G_8 - G_m G_m) I^m(q^2) - G_m\}, \quad (10)$$

$$C(q^2) = \frac{2}{\det \mathbf{D}(q^2)} \{2(G_0 G_8 - G_m G_m) I^8(q^2) - G_0\}, \quad (11)$$

and

$$G_0 = \frac{1}{2}G_S - \frac{1}{3}(2\langle\bar{u}u\rangle + \langle\bar{s}s\rangle)G_D, \quad (12)$$

$$G_8 = \frac{1}{2}G_S - \frac{1}{6}(\langle\bar{s}s\rangle - 4\langle\bar{u}u\rangle)G_D, \quad (13)$$

$$G_m = -\frac{1}{3\sqrt{2}}(\langle\bar{s}s\rangle - \langle\bar{u}u\rangle)G_D. \quad (14)$$

The quark-antiquark bubble integrals are

$$I^0(q^2) = i \int^\Lambda \frac{d^4p}{(2\pi)^4} \text{Tr}^{(c,f,D)}[S_F(p)\lambda^0 i\gamma_5 S_F(p+q)\lambda^0 i\gamma_5], \quad (15)$$

$$I^8(q^2) = i \int^\Lambda \frac{d^4p}{(2\pi)^4} \text{Tr}^{(c,f,D)}[S_F(p)\lambda^8 i\gamma_5 S_F(p+q)\lambda^8 i\gamma_5], \quad (16)$$

$$I^m(q^2) = i \int^\Lambda \frac{d^4p}{(2\pi)^4} \text{Tr}^{(c,f,D)}[S_F(p)\lambda^0 i\gamma_5 S_F(p+q)\lambda^8 i\gamma_5], \quad (17)$$

with $q = p_1 + p_2$. The 2×2 matrix \mathbf{D} is

$$\mathbf{D}(q^2) = \begin{pmatrix} D_{11}(q^2) & D_{12}(q^2) \\ D_{21}(q^2) & D_{22}(q^2) \end{pmatrix}, \quad (18)$$

with

$$D_{11}(q^2) = 2G_8 I^8(q^2) + 2G_m I^m(q^2) - 1, \quad (19)$$

$$D_{12}(q^2) = 2G_8 I^m(q^2) + 2G_m I^0(q^2), \quad (20)$$

$$D_{21}(q^2) = 2G_0 I^m(q^2) + 2G_m I^8(q^2), \quad (21)$$

$$D_{22}(q^2) = 2G_0 I^0(q^2) + 2G_m I^m(q^2) - 1. \quad (22)$$

From the pole position of the scattering amplitude Eq. (8), the η -meson mass m_η is determined.

The scattering amplitude Eq. (8) can be diagonalized by rotation in the flavor space

$$\begin{aligned} \mathcal{T}_{q\bar{q}} &= - \begin{pmatrix} \bar{u}(p_3) \lambda^8 i \gamma_5 v(p_4) \\ \bar{u}(p_3) \lambda^0 i \gamma_5 v(p_4) \end{pmatrix}^T \mathbf{T}_\theta^{-1} \mathbf{T}_\theta \begin{pmatrix} A(q^2) & B(q^2) \\ B(q^2) & C(q^2) \end{pmatrix} \mathbf{T}_\theta^{-1} \\ &\quad \times \mathbf{T}_\theta \begin{pmatrix} \bar{v}(p_2) \lambda^8 i \gamma_5 u(p_1) \\ \bar{v}(p_2) \lambda^0 i \gamma_5 u(p_1) \end{pmatrix}, \end{aligned} \quad (23)$$

$$\begin{aligned} &= - \begin{pmatrix} \bar{u}(p_3) \lambda^\eta i \gamma_5 v(p_4) \\ \bar{u}(p_3) \lambda^{\eta'} i \gamma_5 v(p_4) \end{pmatrix}^T \begin{pmatrix} D^\eta(q^2) & 0 \\ 0 & D^{\eta'}(q^2) \end{pmatrix} \\ &\quad \times \begin{pmatrix} \bar{v}(p_2) \lambda^\eta i \gamma_5 u(p_1) \\ \bar{v}(p_2) \lambda^{\eta'} i \gamma_5 u(p_1) \end{pmatrix}, \end{aligned} \quad (24)$$

with $\lambda^\eta \equiv \cos \theta \lambda^8 - \sin \theta \lambda^0$, $\lambda^{\eta'} \equiv \sin \theta \lambda^8 + \cos \theta \lambda^0$ and

$$\mathbf{T}_\theta = \begin{pmatrix} \cos \theta & -\sin \theta \\ \sin \theta & \cos \theta \end{pmatrix}. \quad (25)$$

The rotation angle θ is determined by

$$\tan 2\theta = \frac{2B(q^2)}{C(q^2) - A(q^2)}. \quad (26)$$

So θ depends on q^2 . At $q^2 = m_\eta^2$, θ represents the mixing angle of the λ^8 and λ^0 components in the η -meson state. In the usual effective pseudoscalar meson lagrangian approaches, the η and η' mesons are analyzed using the q^2 -independent η - η' mixing angle. Because of the q^2 -dependence, θ cannot be interpreted as the

η - η' mixing angle. The origin of the q^2 -dependence is that the η and η' meson have the internal quark structures.

For the η' meson, since the NJL model does not confine quarks, the η' -meson state has the unphysical imaginary part which corresponds to the $\eta' \rightarrow q\bar{q}$ decays. Therefore we do not apply our model to the η' meson in this article.

We define the effective η -quark coupling constant g_η by introducing additional vertex lagrangian,

$$\mathcal{L}_{\eta qq} = g_\eta \bar{\psi} i\gamma_5 \lambda^\eta \psi \phi_\eta, \quad (27)$$

with $\lambda^\eta = \cos \theta \lambda^8 - \sin \theta \lambda^0$. Here ϕ is an auxiliary meson field introduced for convenience and the effective η -quark coupling constant is calculated from the residue of the $q\bar{q}$ -scattering amplitudes at the η pole, i.e. $g_\eta^2 = \lim_{q^2 \rightarrow m_\eta^2} (q^2 - m_\eta^2) D_\eta(q^2)$. The η decay constant f_η is determined by calculating the quark-antiquark one-loop graph,

$$f_\eta = \frac{g_\eta}{m_\eta^2} \int^\Lambda \frac{d^4 p}{(2\pi)^4} \text{Tr}^{(c,f,D)} [q^\mu \gamma_\mu \gamma_5 \frac{\lambda^\eta}{2} S_F(p) i\gamma_5 \lambda^\eta S_F(p-q)] \Big|_{q^2=m_\eta^2}. \quad (28)$$

One can easily show that in the $U_A(1)$ limit, i.e., $G_D = 0$ and $m_{u,d} \neq m_s$, the η meson becomes the ideal mixing state composed of u and d-quarks, namely, $m_\eta = m_\pi$, $g_\eta = g_\pi$, $f_\eta = f_\pi$ and $\tan \theta = -\sqrt{2}$.

3 η -meson decays

3.1 $\eta \rightarrow \gamma\gamma$ decay

The $P \rightarrow \gamma\gamma$ ($P = \pi^0, \eta, \eta'$) decay amplitude is given by

$$\langle \gamma(k_1) \gamma(k_2) | P(p) \rangle = i(2\pi)^4 \delta^4(k_1 + k_2 - p) \varepsilon_{\mu\nu\rho\sigma} \epsilon_1^\mu \epsilon_2^\nu k_1^\rho k_2^\sigma \tilde{\mathcal{T}}_{P \rightarrow \gamma\gamma}(p^2), \quad (29)$$

where ϵ_1 and ϵ_2 are the polarization vectors of the photon and the $P \rightarrow \gamma\gamma$ decay width $\Gamma(P \rightarrow \gamma\gamma)$ is given by

$$\Gamma(P \rightarrow \gamma\gamma) = \left| \tilde{\mathcal{T}}_{P \rightarrow \gamma\gamma} \right|^2 \frac{m_P^3}{64\pi}. \quad (30)$$

In the analysis of the η - η' mixing angle, the $\eta, \eta' \rightarrow \gamma\gamma$ decay widths and the current algebra formulae are used [27]. In order to see the assumptions used in the derivation of the current algebra formulae for the $\eta, \eta' \rightarrow \gamma\gamma$ decay amplitudes, we re-derive them here.

The starting points are the following PCAC relations which are modified by the ABJ anomaly.

$$\partial^\mu A_\mu^8 = f_{8\eta} m_\eta^2 \phi_\eta + f_{8\eta'} m_{\eta'}^2 \phi_{\eta'} - \frac{\alpha}{4\pi} N_c D^8 \varepsilon_{\mu\nu\rho\sigma} F^{\mu\nu} F^{\rho\sigma} , \quad (31)$$

$$\partial^\mu A_\mu^0 = f_{0\eta} m_\eta^2 \phi_\eta + f_{0\eta'} m_{\eta'}^2 \phi_{\eta'} - \frac{\alpha}{4\pi} N_c D^0 \varepsilon_{\mu\nu\rho\sigma} F^{\mu\nu} F^{\rho\sigma} . \quad (32)$$

with

$$\begin{aligned} \langle 0 | \partial^\mu A_\mu^8 | \eta \rangle &= f_{8\eta} m_\eta^2 , & \langle 0 | \partial^\mu A_\mu^8 | \eta' \rangle &= f_{8\eta'} m_{\eta'}^2 , \\ \langle 0 | \partial^\mu A_\mu^0 | \eta \rangle &= f_{0\eta} m_\eta^2 , & \langle 0 | \partial^\mu A_\mu^0 | \eta' \rangle &= f_{0\eta'} m_{\eta'}^2 , \end{aligned} \quad (33)$$

and D^a ($a = 3, 8, 0$) is defined as $\text{tr}[\{Q, Q\} \frac{\lambda^a}{2}]$ with $Q \equiv \frac{1}{2}(\lambda^3 + \frac{1}{\sqrt{3}}\lambda^8)$. α is the fine structure constant of QED and $F^{\mu\nu}$ is the electromagnetic field tensor. The simple η - η' state mixing is then assumed, i.e.,

$$\begin{cases} |\eta\rangle = \cos\theta |\eta_8\rangle - \sin\theta |\eta_0\rangle , \\ |\eta'\rangle = \sin\theta |\eta_8\rangle + \cos\theta |\eta_0\rangle , \end{cases} \quad (34)$$

and

$$\langle 0 | \partial^\mu A_\mu^8 | \eta_8 \rangle = f_8 m_{\eta_8}^2 , \quad \langle 0 | \partial^\mu A_\mu^0 | \eta_0 \rangle = f_0 m_{\eta_0}^2 . \quad (35)$$

From Eqs. (33)-(35), $f_{8\eta} = f_8 \cos\theta$, $f_{8\eta'} = f_8 \sin\theta$, $f_{0\eta} = -f_0 \sin\theta$ and $f_{0\eta'} = f_0 \cos\theta$ are obtained. The η -meson field ϕ_η is expressed as follows.

$$\begin{aligned} \phi_\eta &= \frac{1}{m_\eta^2} \left(\frac{\cos\theta}{f_8} \partial^\mu A_\mu^8 - \frac{\sin\theta}{f_0} \partial^\mu A_\mu^0 \right) \\ &\quad + \frac{\alpha}{4\pi} \varepsilon_{\mu\nu\rho\sigma} F^{\mu\nu} F^{\rho\sigma} \frac{1}{m_\eta^2} \left(\frac{\cos\theta}{f_8} \frac{1}{2\sqrt{3}} - \frac{\sin\theta}{f_0} \sqrt{\frac{2}{3}} \right) . \end{aligned} \quad (36)$$

Using the LSZ-reduction formula, the $\eta \rightarrow \gamma\gamma$ decay amplitude is given by

$$\begin{aligned} T_{\eta \rightarrow \gamma\gamma} &\equiv \langle \gamma(k_1) \gamma(k_2) | \eta(p) \rangle \\ &= i \int d^4x e^{-ip \cdot x} (\square + m_\eta^2) \langle \gamma(k_1) \gamma(k_2) | \phi_\eta(x) | 0 \rangle . \end{aligned} \quad (37)$$

By inserting modified PCAC relation Eq. (36),

$$T_{\eta \rightarrow \gamma\gamma} = \lim_{p^2 \rightarrow m_\eta^2} \left[T_{\eta \rightarrow \gamma\gamma}^{(1)}(p^2) + T_{\eta \rightarrow \gamma\gamma}^{(2)}(p^2) \right] , \quad (38)$$

with

$$T_{\eta \rightarrow \gamma\gamma}^{(1)}(p^2) = \frac{(m_\eta^2 - p^2)}{m_\eta^2} i \int d^4x e^{-ip \cdot x}$$

$$\times \left\langle \gamma(k_1) \gamma(k_2) \left| \mathcal{T} \left[\frac{\cos \theta}{f_8} \partial^\mu A_\mu^8 - \frac{\sin \theta}{f_0} \partial^\mu A_\mu^0 \right] \right| 0 \right\rangle, \quad (39)$$

$$\begin{aligned} T_{\eta \rightarrow \gamma\gamma}^{(2)}(p^2) &= \frac{(m_\eta^2 - p^2)}{m_\eta^2} i \int d^4x e^{-ip \cdot x} \left(\frac{\cos \theta}{f_8} \frac{1}{2\sqrt{3}} - \frac{\sin \theta}{f_0} \sqrt{\frac{2}{3}} \right) \\ &\times \left\langle \gamma(k_1) \gamma(k_2) \left| \mathcal{T} \left[\frac{\alpha}{4\pi} \varepsilon_{\mu\nu\rho\sigma} F^{\mu\nu} F^{\rho\sigma} \right] \right| 0 \right\rangle. \end{aligned} \quad (40)$$

Using the current algebra techniques and from the consideration of the general structure of the matrix element, we can show that $T_{\eta \rightarrow \gamma\gamma}^{(1)}(p^2 = 0) = 0$ [28]. $T_{\eta \rightarrow \gamma\gamma}^{(2)}$ can be calculated easily,

$$\begin{aligned} T_{\eta \rightarrow \gamma\gamma}^{(2)}(p^2) &= i (2\pi)^4 \delta^4(k_1 + k_2 - p) \varepsilon_{\mu\nu\rho\sigma} \epsilon_1^\mu \epsilon_2^\nu k_1^\rho k_2^\sigma \frac{(m_\eta^2 - p^2)}{m_\eta^2} \\ &\times \frac{\alpha}{\pi} \frac{1}{\sqrt{3}} \left(\frac{\cos \theta}{f_8} - 2\sqrt{2} \frac{\sin \theta}{f_0} \right), \end{aligned} \quad (41)$$

therefore the reduced invariant amplitude $\tilde{\mathcal{T}}_{\eta \rightarrow \gamma\gamma}$ in the soft η limit is

$$\tilde{\mathcal{T}}_{\eta \rightarrow \gamma\gamma}(p^2 = 0) = \frac{\alpha}{\pi} \frac{1}{\sqrt{3}} \left(\frac{\cos \theta}{f_8} - 2\sqrt{2} \frac{\sin \theta}{f_0} \right). \quad (42)$$

Similarly, the reduced invariant amplitude $\tilde{\mathcal{T}}_{\eta' \rightarrow \gamma\gamma}$ in the soft η' limit is

$$\tilde{\mathcal{T}}_{\eta' \rightarrow \gamma\gamma}(p^2 = 0) = \frac{\alpha}{\pi} \frac{1}{\sqrt{3}} \left(\frac{\sin \theta}{f_8} + 2\sqrt{2} \frac{\cos \theta}{f_0} \right). \quad (43)$$

Finally, $\tilde{\mathcal{T}}_{\eta \rightarrow \gamma\gamma}(p^2 = 0) \simeq \tilde{\mathcal{T}}_{\eta \rightarrow \gamma\gamma}(p^2 = m_\eta^2)$ and $\tilde{\mathcal{T}}_{\eta' \rightarrow \gamma\gamma}(p^2 = 0) \simeq \tilde{\mathcal{T}}_{\eta' \rightarrow \gamma\gamma}(p^2 = m_{\eta'}^2)$ are assumed in the usual analysis of the η - η' mixing angle [27]. Since m_η and $m_{\eta'}$ are not significantly smaller than the typical hadronic mass scale, the above results should not be taken quantitatively. Furthermore, because of the ABJ anomaly by the gluons ($U_A(1)$ anomaly) in the flavor singlet channel, the saturation of the flavor singlet axialvector current by the η and η' field is rather questionable.

In the NJL model, the on meson mass shell $\pi^0, \eta \rightarrow \gamma\gamma$ decay amplitudes can be obtained by calculating the quark triangle diagrams shown in Fig. 1 and our results are

$$\tilde{\mathcal{T}}_{\pi^0 \rightarrow \gamma\gamma}(p^2 = m_{\pi^0}^2) = \frac{\alpha}{\pi} g_\pi F_{\pi^0}^u, \quad (44)$$

$$\begin{aligned} \tilde{\mathcal{T}}_{\eta \rightarrow \gamma\gamma}(p^2 = m_\eta^2) &= \frac{\alpha}{\pi} g_\eta \frac{1}{3\sqrt{3}} \left[\cos \theta \left\{ 5F_\eta^u - 2F_\eta^s \right\} \right. \\ &\quad \left. - \sin \theta \sqrt{2} \left\{ 5F_\eta^u + F_\eta^s \right\} \right]. \end{aligned} \quad (45)$$

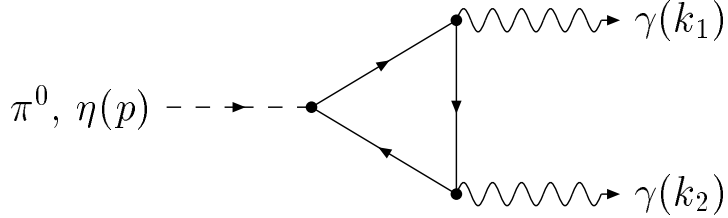


Figure 1: The quark triangle diagram for $\pi^0, \eta \rightarrow \gamma\gamma$ decays.

Here F_P^a ($a = u, s$ and $P = \pi^0, \eta$) is defined as

$$\begin{aligned} F_P^a &= \int_0^1 dx \int_0^1 dy \frac{2(1-x)M_a}{M_a^2 - m_P^2 x(1-x)(1-y)} \\ &= \frac{4M_a}{m_P^2} \arcsin^2 \left(\frac{m_P}{2M_a} \right). \end{aligned} \quad (46)$$

We can see that the integrand of F_P^a has an unphysical pole when $m_P \geq 2M_a$. It is due to lack of the confinement mechanism in the NJL model.

In the chiral limit, the pion mass vanishes and $F_{\pi^0}^u$ becomes $1/M_u$. In this limit, the Goldberger-Treiman (GT) relation at the quark level, $M_u = g_\pi f_\pi$, holds in the NJL model and this leads to $\tilde{T}_{\pi^0 \rightarrow \gamma\gamma} = \alpha/(\pi f_\pi)$ which is same as the tree-level results in the Wess-Zumino-Witten lagrangian approach [4, 5]. It should be mentioned that we have to integrate out the triangle diagrams without introducing a cutoff Λ in order to get the above result though the cutoff is introduced in the gap equations in the NJL model. In the $U(3)_L \times U(3)_R$ version of the NJL model, the WZW term has been derived using the bosonization method with the heat-kernel expansion [29, 30]. In their approach, $O(1/\Lambda)$ term has been neglected and it is equivalent to taking the $\Lambda \rightarrow \infty$ limit.

3.2 $\eta \rightarrow \gamma l^- l^+$ decays

The $P \rightarrow \gamma l^- l^+$ ($P = \pi^0, \eta$ and $l = e, \mu$) decay amplitude is given by

$$\begin{aligned} \langle \gamma(k) l^-(q_1) l^+(q_2) | P(p) \rangle &= i(2\pi)^4 \delta^4(q_1 + q_2 + k - p) \\ &\quad \times \varepsilon_{\mu\nu\rho\sigma} e \bar{u}(q_1) \gamma^\mu v(q_2) \frac{1}{q^2} k^\rho q^\sigma \tilde{T}_{P \rightarrow \gamma l^- l^+}(q^2), \end{aligned} \quad (47)$$

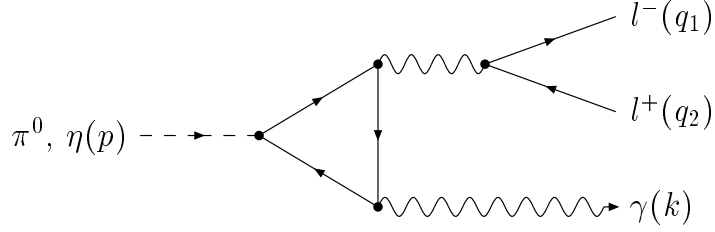


Figure 2: The quark triangle diagram for $\pi^0, \eta \rightarrow \gamma l^- l^+$ decays.

where $q \equiv q_1 + q_2$ and u and v denotes lepton and antilepton's spinors. The lepton pair invariant mass square spectrum is

$$\frac{d\Gamma(P \rightarrow \gamma l^- l^+)}{dx} = \frac{\alpha}{96\pi^2} m_P^3 \frac{(1-x)^3}{x} \left(1 - \frac{r^2}{x}\right)^{\frac{1}{2}} \left(1 + \frac{r^2}{2x}\right) \times |\tilde{\mathcal{T}}_{P \rightarrow \gamma l^- l^+}(m_P^2 x)|^2, \quad \text{with } (1 \geq x \geq r^2). \quad (48)$$

Here $x \equiv q^2/m_P^2$ and $r \equiv 2m_l/m_P$ and the total $P \rightarrow \gamma l^- l^+$ decay width is given by

$$\begin{aligned} & \Gamma(P \rightarrow \gamma l^- l^+) \\ &= \frac{\alpha}{96\pi^2} m_P^3 \int_{r^2}^1 dx \frac{(1-x)^3}{x} \left(1 - \frac{r^2}{x}\right)^{\frac{1}{2}} \left(1 + \frac{r^2}{2x}\right) |\tilde{\mathcal{T}}_{P \rightarrow \gamma l^- l^+}(m_P^2 x)|^2. \end{aligned} \quad (49)$$

By calculating the diagram shown in Fig. 2, we obtain the $\pi^0, \eta \rightarrow \gamma l^- l^+$ decay amplitudes as follows.

$$\tilde{\mathcal{T}}_{\pi^0 \rightarrow \gamma l^- l^+}(q^2) = \frac{\alpha}{\pi} g_\pi G_\pi^u(q^2) \quad (50)$$

$$\begin{aligned} \tilde{\mathcal{T}}_{\eta \rightarrow \gamma l^- l^+}(q^2) &= \frac{\alpha}{\pi} g_\eta \frac{1}{3\sqrt{3}} \left[\cos \theta \left\{ 5G_\eta^u(q^2) - 2G_\eta^s(q^2) \right\} \right. \\ &\quad \left. - \sin \theta \sqrt{2} \left\{ 5G_\eta^u(q^2) + G_\eta^s(q^2) \right\} \right], \end{aligned} \quad (51)$$

where

$$\begin{aligned} G_P^a(q^2) &= \int_0^1 dx \int_0^1 dy \frac{2(1-x)M_a}{M_a^2 - m_P^2 x(1-x)(1-y) - q^2 x(1-x)y} \\ &= \frac{4M_a}{(m_P^2 - q^2)} \left\{ \arcsin^2 \left(\frac{m_P}{2M_a} \right) - \arcsin^2 \left(\frac{q}{2M_a} \right) \right\}, \end{aligned} \quad (52)$$

with $q \equiv \sqrt{q^2}$. We can find the following relations, $G_P^a(q^2 = 0) = F_P^a$ and $\tilde{\mathcal{T}}_{P \rightarrow \gamma l^- l^+}(q^2 = 0) = \tilde{\mathcal{T}}_{P \rightarrow \gamma\gamma}$.

From the observed data for the two-photon transition $\gamma\gamma^* \rightarrow P$ and the lepton pair invariant mass spectrum of the $P \rightarrow \gamma l^- l^+$ decay, one can obtain the $P\gamma\gamma^*$ transition form factor $f_{P\gamma\gamma^*}(q^2)$ defined by

$$f_{P\gamma\gamma^*}(q^2) \equiv \frac{\tilde{\mathcal{T}}_{P \rightarrow \gamma l^- l^+}(q^2)}{\tilde{\mathcal{T}}_{P \rightarrow \gamma\gamma}(q^2 = 0)}. \quad (53)$$

For the spacelike q^2 , $G_P^a(q^2)$ is given by

$$G_P^a(q^2) = \frac{2M_a}{(m_P^2 - q^2)} \left\{ 2 \arcsin^2 \left(\frac{m_P}{2M_a} \right) + \frac{1}{2} \ln^2 \frac{\beta + 1}{\beta - 1} \right\}, \quad (54)$$

with $\beta = \sqrt{1 - 4M_a^2/q^2}$. We introduce the slope parameter Λ_P by

$$\frac{1}{\Lambda_P^2} \equiv \left. \frac{d}{dq^2} f_{P\gamma\gamma^*}(q^2) \right|_{q^2=0} \equiv \frac{r_P^2}{6}, \quad (55)$$

and Λ_P corresponds to the pole mass if one fits the q^2 -dependence of $f_{P\gamma\gamma^*}(q^2)$ by means of a single-pole term. In the case of the charge form factor $f_c(q^2)$ of the charged pseudoscalar meson, $6/\Lambda_c^2 \equiv 6df_c(q^2)/dq^2 = \langle r_c^2 \rangle$ is the mean square charge radius of the charged pseudoscalar meson. Therefore, it is natural to consider that Λ_P is related to the size of the neutral pseudoscalar meson P .

Λ_π can be calculated easily in the chiral limit. Using Eqs. (50), (52) and (55), we get $\Lambda_\pi = \sqrt{12}M_u$. On the other hand, the NJL model predicts $\Lambda_c = 2\sqrt{2}f_\pi$ for the pion in the chiral limit [31]. Since Λ_π is expressed in terms of the dynamical quantity of the model: M_u in contrast with Λ_c which is expressed in terms of the observed quantity: f_π , the $P\gamma\gamma^*$ transition form factor may be more sensitive to the dynamical structure of the pseudoscalar meson than the charge form factor.

3.3 $\eta \rightarrow \pi^0\gamma\gamma$ decay

The $\eta \rightarrow \pi^0\gamma\gamma$ decay amplitude is given by

$$\langle \pi^0(p_\pi) \gamma(k_1, \epsilon_1) \gamma(k_2, \epsilon_2) | \eta(p) \rangle = i(2\pi)^4 \delta^4(p_\pi + k_1 + k_2 - p) \epsilon_1^\mu \epsilon_2^\nu T_{\mu\nu}. \quad (56)$$

The dominant contributions to this process in this model are the quark-box diagrams given in Fig. 3. Following the evaluation of the quark-box diagrams

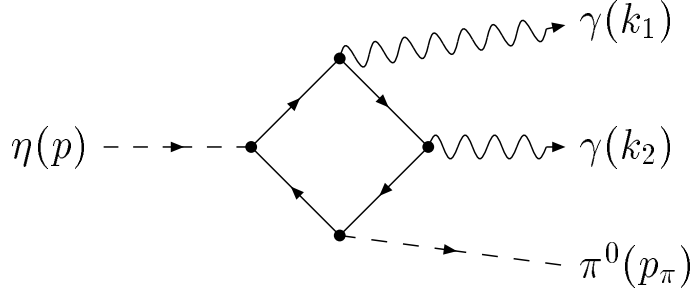


Figure 3: The quark box diagram for $\eta \rightarrow \pi^0 \gamma \gamma$ decay.

performed in [32], we obtain

$$T_{\mu\nu} = -i \frac{1}{\sqrt{3}} (\cos \theta - \sqrt{2} \sin \theta) e^2 g_\eta g_\pi \int \frac{d^4 q}{(2\pi)^4} \sum_{i=1}^6 U_{\mu\nu}^i, \quad (57)$$

with

$$\begin{aligned} U_{\mu\nu}^1 &= \text{tr} \left\{ \gamma_5 \frac{1}{\not{q} - M + i\epsilon} \gamma_5 \frac{1}{\not{q} + \not{p} - \not{k}_1 - \not{k}_2 - M + i\epsilon} \right. \\ &\quad \times \left. \gamma_\nu \frac{1}{\not{q} + \not{p} - \not{k}_1 - M + i\epsilon} \gamma_\mu \frac{1}{\not{q} + \not{p} - M + i\epsilon} \right\}, \end{aligned} \quad (58)$$

$$\begin{aligned} U_{\mu\nu}^2 &= \text{tr} \left\{ \gamma_5 \frac{1}{\not{q} - M + i\epsilon} \gamma_5 \frac{1}{\not{q} + \not{k}_2 - M + i\epsilon} \right. \\ &\quad \times \left. \gamma_\nu \frac{1}{\not{q} + \not{p} - \not{k}_1 - M + i\epsilon} \gamma_\mu \frac{1}{\not{q} + \not{p} - M + i\epsilon} \right\}, \end{aligned} \quad (59)$$

$$\begin{aligned} U_{\mu\nu}^3 &= \text{tr} \left\{ \gamma_5 \frac{1}{\not{q} - M + i\epsilon} \gamma_\nu \frac{1}{\not{q} + \not{k}_2 - M + i\epsilon} \right. \\ &\quad \times \left. \gamma_\mu \frac{1}{\not{q} + \not{k}_1 + \not{k}_2 - M + i\epsilon} \gamma_5 \frac{1}{\not{q} + \not{p} - M + i\epsilon} \right\}, \end{aligned} \quad (60)$$

$$U_{\mu\nu}^4 = U_{\nu\mu}^1(k_1 \leftrightarrow k_2), \quad (61)$$

$$U_{\mu\nu}^5 = U_{\nu\mu}^2(k_1 \leftrightarrow k_2), \quad (62)$$

$$U_{\mu\nu}^6 = U_{\nu\mu}^3(k_1 \leftrightarrow k_2). \quad (63)$$

Here M is the constituent u,d-quark mass. Because the loop integration in (57) is not divergent, we again do not use the UV cutoff. Then the gauge invariance is preserved. The inclusion of the cutoff that is consistent with the gap equation

will break the gauge invariance and make the present calculation too complicated. Note that the strange quark does not contribute to the loop.

On the other hand the amplitude $T_{\mu\nu}$ has a general form required by the gauge invariance [33]

$$\begin{aligned} T^{\mu\nu} &= A(x_1, x_2)(k_1^\nu k_2^\mu - k_1 \cdot k_2 g^{\mu\nu}) \\ &+ B(x_1, x_2) \left[-m_\eta^2 x_1 x_2 g^{\mu\nu} - \frac{k_1 \cdot k_2}{m_\eta^2} p^\mu p^\nu + x_1 k_2^\mu p^\nu + x_2 p^\mu k_1^\nu \right], \end{aligned} \quad (64)$$

with $x_i = p \cdot k_i / m_\eta^2$. With A and B , the differential decay rate with respect to the energies of the two photons is given by

$$\begin{aligned} \frac{d^2\Gamma}{dx_1 dx_2} &= \frac{m_\eta^5}{256\pi^2} \left\{ \left| A + \frac{1}{2}B \right|^2 \left[2(x_1 + x_2) + \frac{m_\pi^2}{m_\eta^2} - 1 \right]^2 \right. \\ &\quad \left. + \frac{1}{4} |B|^2 \left[4x_1 x_2 - \left[2(x_1 + x_2) + \frac{m_\pi^2}{m_\eta^2} - 1 \right] \right]^2 \right\}. \end{aligned} \quad (65)$$

Though the mass of η as a $\bar{q}q$ bound state depends on G_D , we use the experimental value $m_\eta = 547$ MeV in evaluating (65). The Dalitz boundary is given by two conditions:

$$\frac{1}{2} \left(1 - \frac{m_\pi^2}{m_\eta^2} \right) \leq x_1 + x_2 \leq 1 - \frac{m_\pi}{m_\eta}, \quad (66)$$

and

$$x_1 + x_2 - 2x_1 x_2 \leq \frac{1}{2} \left(1 - \frac{m_\pi^2}{m_\eta^2} \right). \quad (67)$$

In evaluating (58)-(63), one only has to identify the coefficients of $p^\mu p^\nu$ and $g^{\mu\nu}$. Details of the calculation are given in [32]. Defining \mathcal{A} and \mathcal{B} by

$$\int \frac{d^4q}{(2\pi)^4} \sum_{i=1}^6 U_i^{\mu\nu} = -i \left(\mathcal{A} g^{\mu\nu} + \mathcal{B} \frac{p^\mu p^\nu}{m_\eta^2} + \dots \right), \quad (68)$$

we find A and B as

$$A = \frac{1}{\sqrt{3}} (\cos \theta - \sqrt{2} \sin \theta) e^2 g_\pi g_\eta \frac{2}{m_\eta^2 \sigma} \left[\mathcal{A} - 2x_1 x_2 \frac{\mathcal{B}}{\sigma} \right], \quad (69)$$

$$B = \frac{1}{\sqrt{3}} (\cos \theta - \sqrt{2} \sin \theta) e^2 g_\pi g_\eta \frac{2}{m_\eta^2 \sigma} \mathcal{B}, \quad (70)$$

with

$$\sigma = \frac{(k_1 + k_2)^2}{m_\eta^2} = 2(x_1 + x_2) + \frac{m_\pi^2}{m_\eta^2} - 1. \quad (71)$$

We evaluate \mathcal{A} and \mathcal{B} numerically and further integrate (65) to obtain the $\eta \rightarrow \pi^0 \gamma \gamma$ decay rate.

4 Numerical results

4.1 η -meson mass, mixing angle and decay constant

We discuss our numerical results of the η -meson mass m_η , mixing angle θ and the η decay constant f_η in this subsection. The parameters of the NJL model are the current quark masses $m_u = m_d$, m_s , the four-quark coupling constant G_S , the $U_A(1)$ breaking six-quark determinant coupling constant G_D and the covariant cutoff Λ . We take G_D as a free parameter and study η meson properties as functions of G_D . We use the light current quark masses $m_u = m_d = 8.0$ MeV to reproduce $M_u = M_d \simeq 330$ MeV ($\simeq 1/3M_N$) which is the value usually used in the nonrelativistic quark model. Other parameters, m_s , G_S and Λ , are determined so as to reproduce the isospin averaged observed masses, $m_\pi = 138.0$ MeV, $m_K = 495.7$ MeV and the pion decay constant $f_\pi = 92.4$ MeV.

We obtain $m_s = 193$ MeV, $\Lambda = 783$ MeV, $M_{u,d} = 325$ MeV and $g_{\pi qq} = 3.44$, which are almost independent of G_D . The ratio of the current s-quark mass to the current u,d-quark mass is $m_s/m_u = 24.1$, which agrees well with $m_s/\hat{m} = 24.4 \pm 1.5$ ($\hat{m} = \frac{1}{2}(m_u + m_d)$) derived from ChPT [34]. The kaon decay constant f_K is the prediction and is almost independent of G_D . We have obtained $f_K = 97$ MeV which is about 14% smaller than the observed value. We consider this is the typical predictive power of the NJL model in the strangeness sector. The quark condensates are also independent of G_D and our results are $\langle \bar{u}u \rangle^{\frac{1}{3}} = -216$ MeV and $\langle \bar{s}s \rangle^{\frac{1}{3}} = -226$ MeV, which give

$$\frac{f_\pi^2 m_\pi^2}{-2m_u \langle \bar{u}u \rangle} = 1.01, \quad \frac{f_K^2 m_K^2}{-\frac{1}{2}(m_u + m_s) \langle \bar{u}u + \bar{s}s \rangle} = 1.06. \quad (72)$$

As reported in the previous studies in the NJL model, the Gell-Mann-Oakes-Renner relations hold well for both the pion and kaon sectors.

We define dimensionless parameters $G_D^{\text{eff}} \equiv -G_D(\Lambda/2\pi)^4 \Lambda N_c^2$ and $G_S^{\text{eff}} \equiv G_S(\Lambda/2\pi)^2 N_c$. The calculated results of the η -meson mass m_η and the mixing angle θ are shown in Fig. 4 and Fig. 5, respectively. When G_D^{eff} is zero, our lagrangian does not cause the flavor mixing and therefore the ideal mixing is achieved. The “ η ” is purely $u\bar{u} + d\bar{d}$ which corresponds to $\theta = -54.7^\circ$ and is degenerate to the pion in this limit.

It may be useful to compare our results with those in the $1/N_C$ expansion approach. In the $1/N_C$ expansion approach, with the inclusion of the $O(1/N_C)$

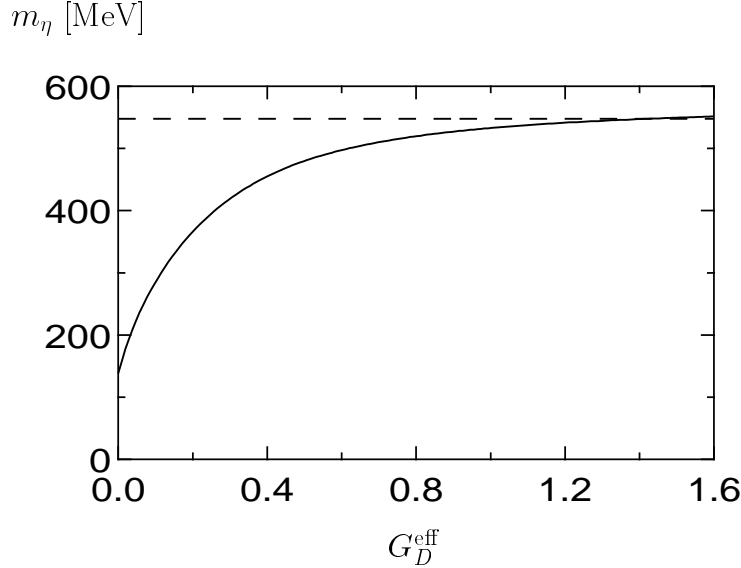


Figure 4: Dependence of the η meson mass on the dimension-less coupling constant G_D^{eff} . The horizontal dashed line indicates the experimental value.

contribution by the $U_A(1)$ anomaly in the flavor singlet-singlet channel, the square mass matrix of the mass term of the low-energy effective lagrangian in the η_8 - η_0 channel becomes as follows [2].

$$M_{\eta-\eta'}^2 = \begin{pmatrix} \frac{4}{3}m_K^2 - \frac{1}{3}m_\pi^2 & -\frac{2}{3}\sqrt{2}(m_K^2 - m_\pi^2) \\ -\frac{2}{3}\sqrt{2}(m_K^2 - m_\pi^2) & \frac{2}{3}m_K^2 + \frac{1}{3}m_\pi^2 + \frac{\chi^2}{N_C} \end{pmatrix}, \quad (73)$$

where

$$\frac{\chi^2}{N_C} \equiv \frac{6}{f_\pi^2}(-i) \int d^4x \partial^\mu \partial^\nu T \langle K_\mu(x) K_\nu(0) \rangle_{YM}. \quad (74)$$

Here the isospin symmetry is assumed and YM means the pure Yang-Mills theory. The ghost field K_μ is defined by

$$\partial^\mu K_\mu \equiv \frac{g^2}{32\pi^2} G_{\mu\nu}^a (\tilde{G}^a)^{\mu\nu}, \quad (75)$$

and $G_{\mu\nu}^a$ is the gluon field strength tensor. By diagonalizing the matrix given in Eq. (73), we obtain

$$m_{\eta,\eta'}^2 = \left(m_K^2 + \frac{\chi^2}{2N_C} \right) \pm \frac{1}{2} \sqrt{\left(2m_K^2 - 2m_\pi^2 - \frac{\chi^2}{3N_C} \right)^2 + \frac{8}{9} \frac{\chi^4}{N_C^2}}, \quad (76)$$

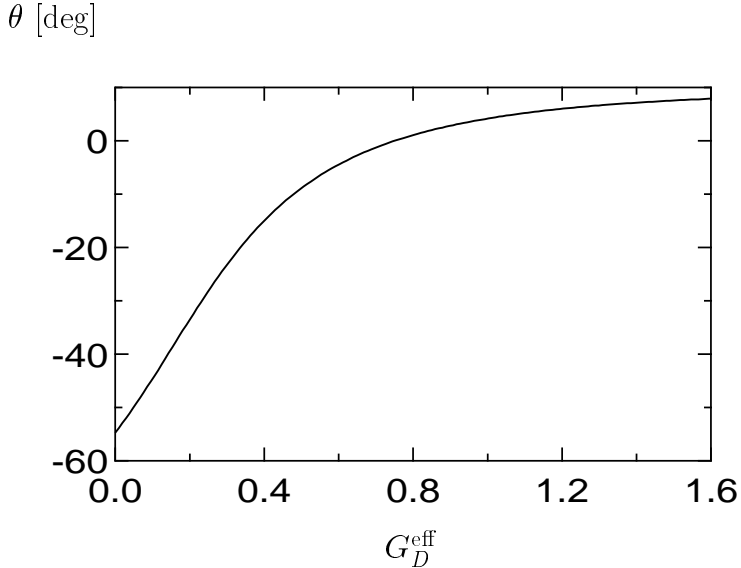


Figure 5: Dependence of the mixing angle θ on the dimension-less coupling constant G_D^{eff} . The horizontal dashed line indicates the experimental value.

and

$$\tan \theta = \frac{\frac{4}{3}m_K^2 - \frac{1}{3}m_\pi^2 - m_\eta^2}{-\frac{2}{3}\sqrt{2}(m_K^2 - m_\pi^2)}. \quad (77)$$

From Eqs. (76) and (77), it is obvious that in the $U_A(1)$ limit the η and η' become the ideal mixing state with $m_\eta = m_\pi \simeq 138$ MeV and $m_{\eta'} = \sqrt{2m_K^2 - m_\pi^2} \simeq 687$ MeV. We compare the dependence of the η meson mass on the mixing angle calculated in the NJL model with that given in Eq. (77) in the $1/N_C$ expansion approach in Fig. 6 and find that the η meson mass calculated in the NJL model is somewhat smaller than that in the $1/N_C$ expansion approach at the same mixing angle (except for the ideal mixing point) though the shapes are similar. The value of the mixing angle is one of the important quantity to understand the physics of the η and η' mesons. The mixing angle determined from the η - η' mass formula is often discussed in the literature. However since the η meson mass is not so sensitive to the mixing angle as shown in Fig. 6, it is not suitable to determine the mixing angle from the η meson mass.

We next discuss the η decay constant f_η . The calculated η decay constant

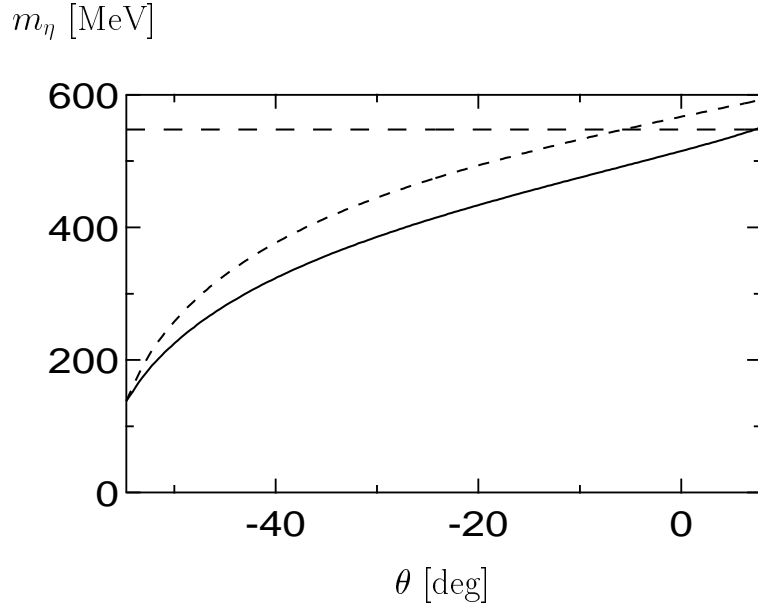


Figure 6: Dependence of the η meson mass on the mixing angle. The solid line indicates the result calculated in the NJL model and the short-dashed line indicates that in the $1/N_C$ expansion approach. The horizontal long-dashed line shows the experimental η meson mass.

is shown in Fig. 7. It is almost independent of G_D and $f_\eta \simeq f_\pi$. For example, $f_\eta = 91.2$ MeV at $G_D^{\text{eff}} = 0.7$. Therefore it seems that the η meson does not lose the Nambu-Goldstone boson nature though its mass and mixing angle are strongly affected by the $U_A(1)$ breaking interaction.

The charged pion and kaon decay constants can be directly obtained by measuring the $\pi \rightarrow \mu\nu_\mu$ and $K \rightarrow \mu\nu_\mu$ decays. On the other hand the decay constants for the light neutral pseudoscalar mesons π^0 , η and η' cannot be obtained from the direct measurements. As discussed in Sect. 3.1, they are related to the $P \rightarrow \gamma\gamma$ decay amplitudes in the soft limit. It is widely accepted that the soft meson limit is close to the on-shell point in the pion case. However it is the matter of discussions how good the soft η and η' limits are. We will discuss this point in the next section by comparing the $\eta \rightarrow \gamma\gamma$ decay amplitude which is directly calculated in the NJL model with that obtained using PCAC + ABJ anomaly in the soft η limit.

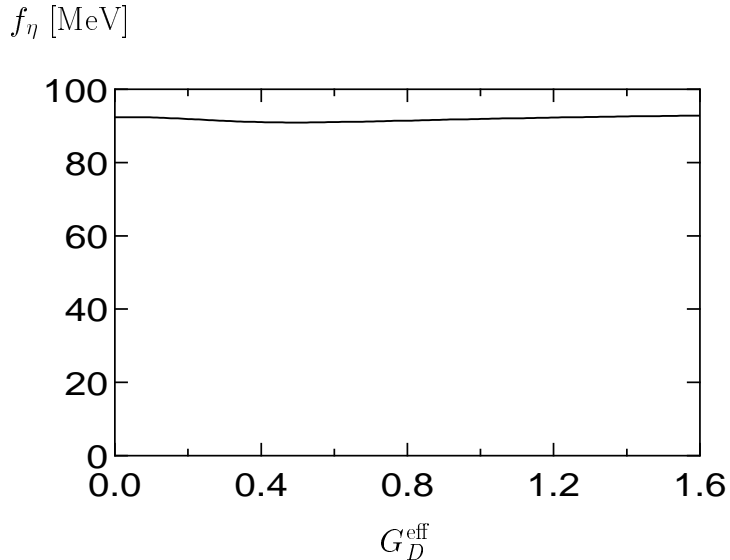


Figure 7: Dependence of the η decay constant f_η on the dimension-less coupling constant G_D^{eff} .

Since the NJL model does not confine quarks, the η' meson is not a bound state. Therefore we do not apply our model to the η' meson. On the contrary, the η meson appears as a bound state. Nevertheless, one may ask whether the present model is applicable to the η meson since the binding energy of the η meson ($2M_u - m_\eta$) is much smaller than those of the pion and kaon. In order to confirm it, we study the constituent u, d-quark mass dependence of the η -meson properties. By changing the current u, d-quark mass $m_{u,d}$ from 7.5 MeV to 8.5 MeV, the constituent u,d-quark mass $M_{u,d}$ is changed from about 300 MeV to 360 MeV. Other parameters of the model are chosen so as to reproduce the experimental values of m_π , m_K , m_η and f_π . This change causes the change of the binding energy of the η meson from about 50 MeV to 170 MeV. The change of the calculated η decay constant is within 2% and the change of the calculated mixing angle is within 12%. This stability of the η -meson properties indicates that the NJL model can describe the essential feature of the η meson.

4.2 $\eta \rightarrow \gamma\gamma$ decay

The recent experimental results of the $\pi^0, \eta \rightarrow \gamma\gamma$ decay widths are $\Gamma(\pi^0 \rightarrow \gamma\gamma) = 7.7 \pm 0.6$ eV and $\Gamma(\eta \rightarrow \gamma\gamma) = 0.510 \pm 0.026$ keV [35] and the reduced amplitudes are

$$|\tilde{\mathcal{T}}_{\pi^0 \rightarrow \gamma\gamma}| = (2.5 \pm 0.1) \times 10^{-11} \text{ [eV]}^{-1}, \quad (78)$$

$$|\tilde{\mathcal{T}}_{\eta \rightarrow \gamma\gamma}| = (2.5 \pm 0.06) \times 10^{-11} \text{ [eV]}^{-1}. \quad (79)$$

Here we have used the two photon measurement result for the $\eta \rightarrow \gamma\gamma$ decay width. From Eq. (44) and Eq. (45), we get $\tilde{\mathcal{T}}_{\eta \rightarrow \gamma\gamma} = (5/3)\tilde{\mathcal{T}}_{\pi^0 \rightarrow \gamma\gamma}$ in the $U_A(1)$ limit. Therefore in order to reproduce the experimental value of $\tilde{\mathcal{T}}_{\eta \rightarrow \gamma\gamma}$, the effect of the $U_A(1)$ anomaly should reduce $\tilde{\mathcal{T}}_{\eta \rightarrow \gamma\gamma}$ by a factor 3/5.

We first discuss the $\pi^0 \rightarrow \gamma\gamma$ decay. The calculated result is $\tilde{\mathcal{T}}_{\pi^0 \rightarrow \gamma\gamma} = 2.50 \times 10^{-11}$ (1/eV) which agrees well with the observed value given in Eq. (78). The current algebra result is $\tilde{\mathcal{T}}_{\pi^0 \rightarrow \gamma\gamma} = \alpha/(\pi f_\pi) = 2.514 \times 10^{-11}$ (1/eV), and thus the soft pion limit is a good approximation for $\pi^0 \rightarrow \gamma\gamma$ decay. The chiral symmetry breaking affects $\tilde{\mathcal{T}}_{\pi^0 \rightarrow \gamma\gamma}$ in two ways. One is the deviation from the G-T relation and another is the matrix element of the triangle diagram $F(u, \pi^0)$. Our numerical results are $g_\pi = 3.44$, $M_u/f_\pi = 3.52$ and $F(u, \pi^0)M_u = 1.015$, therefore the deviations from the soft pion limit are very small both in the G-T relation and the matrix element of the triangle diagram.

Let us now turn to the discussion of the $\eta \rightarrow \gamma\gamma$ decay. The calculated results of the $\eta \rightarrow \gamma\gamma$ decay amplitude $\tilde{\mathcal{T}}_{\eta \rightarrow \gamma\gamma}$ is given in Fig. 8. The experimental value of the $\eta \rightarrow \gamma\gamma$ decay amplitude is reproduced at about $G_D^{\text{eff}} = 0.7$. The calculated η -meson mass at $G_D^{\text{eff}} = 0.7$ is $m_\eta = 510$ MeV which is 7% smaller than the observed mass. As for the effects of the symmetry breaking on $\tilde{\mathcal{T}}_{\eta \rightarrow \gamma\gamma}$, our results are $F(u, \eta) M_u = 1.36$ and $F(u, \eta)/F(s, \eta) = 1.99$ at $G_D^{\text{eff}} = 0.7$. Therefore it seems that the soft η limit is not close to the real world in this case. Recently, Bernard et al. [36] calculated the $\eta \rightarrow \gamma\gamma$ decay width using a similar model. They used a rather weak instanton induced interaction and their result of $\Gamma(\eta \rightarrow \gamma\gamma)$ is about 50% bigger than the experimental value. It is understandable from our analysis.

$G_D^{\text{eff}} = 0.7$ corresponds to $G_D \langle \bar{s}s \rangle / G_S = 0.44$, suggesting that the contribution from \mathcal{L}_6 to the dynamical mass of the up and down quarks is 44% of that from \mathcal{L}_4 . In the previous study of the η and η' mesons in the three-flavor NJL model [16–21],

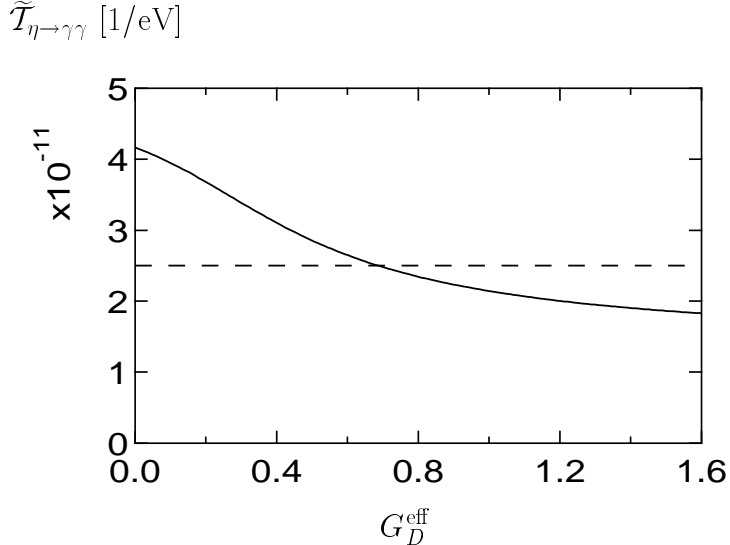


Figure 8: Dependence of the $\eta \rightarrow \gamma\gamma$ decay amplitude on the dimension-less coupling constant G_D^{eff} . The horizontal dashed line indicates the experimental value.

the strength of the instanton induced interaction has been determined so as to reproduce the observed η' mass though the η' state has the unphysical decay mode of the $\eta' \rightarrow \bar{u}u, \bar{d}d$. The strength determined from the η' is much smaller than $G_D^{\text{eff}} = 0.7$, about 1/4 of the present case. One of the shortcomings of the NJL model is the lack of the confinement mechanism. It is expected that the confinement gives rise to the attractive force between quark and antiquark in the η' meson to prevent the η' meson from decaying to the quark and antiquark pair.

In the PCAC + ABJ anomaly approach, if one assumes the $SU(3)$ symmetry, i.e., $f_8 = f_\pi$, and using Eqs. (42) and (43), the mixing angle θ and the meson decay constant in the flavor singlet channel f_0 can be determined so as to reproduce the observed $\Gamma(\eta \rightarrow \gamma\gamma)$ and $\Gamma(\eta' \rightarrow \gamma\gamma)$. The results are $\theta = -17.4^\circ$ and $f_0/f_\pi = 1.1$. The pion and kaon loop corrections are then included in ChPT [6] and the results are $\theta = -21.8^\circ$, $f_8/f_\pi = 1.25$ and $f_0/f_\pi = 1.07$.

In the NJL model, the mixing angle at $G_D^{\text{eff}} = 0.7$ is $\theta = -1.3^\circ$ and that indicates a strong OZI violation and a large (u,d)-s mixing. This disagrees with the “standard” value $\theta \simeq -20^\circ$ obtained in the PCAC + ABJ anomaly approach and ChPT. One of the origin of the difference is that the mixing angle in the NJL

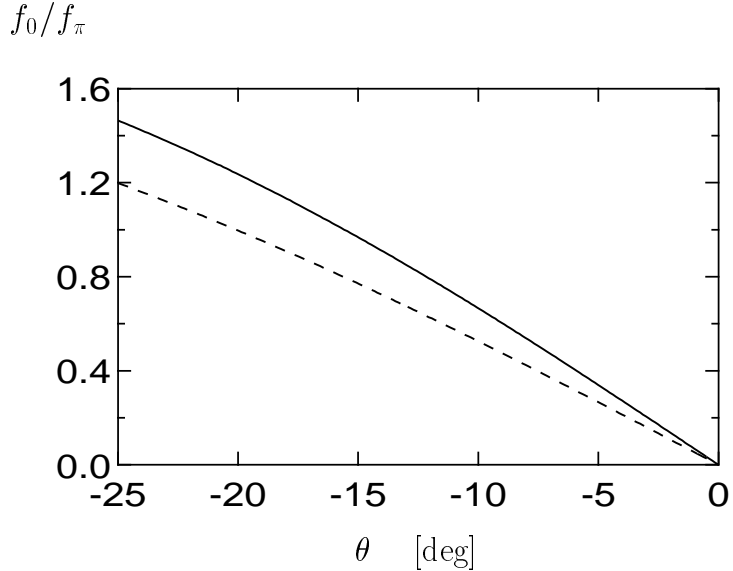


Figure 9: The flavor singlet decay constant f_0 which is determined so as to reproduce the observed $\eta \rightarrow \gamma\gamma$ decay width as a function of θ using the formula derived in the PCAC + ABJ anomaly approach. The solid line indicates in the case of $f_8 = f_\pi$ and the dashed line indicates in the case of $f_8 = 1.25 f_\pi$.

model depends on p^2 of the $\bar{q}q$ state and thus reflects the internal structure of the η meson. On the contrary the analyses in the PCAC + ABJ anomaly approach and ChPT assume an energy-independent mixing angle, i.e., $\theta(p^2 = m_\eta^2) = \theta(p^2 = m_{\eta'}^2)$. Another point is that the $SU(3)$ breaking of the $\eta \rightarrow \gamma\gamma$ decay amplitude is rather large in the NJL model as we have shown above. It indicates that the soft η and η' limits used in the PCAC + ABJ anomaly approach are not so good. In the ChPT point of view, it suggests that the tree diagram contributions from $O(p^6)$ terms may be rather large.

If the PCAC + ABJ anomaly approach is considered not to be applied for the $\eta' \rightarrow \gamma\gamma$ decay, then one cannot determine the mixing angle θ and the flavor singlet decay constant f_0 from the observed $\eta, \eta' \rightarrow \gamma\gamma$ decay widths. However the relation between θ and f_0 can be obtained from Eq. (42) only by the $\eta \rightarrow \gamma\gamma$ decay amplitudes assuming that f_8 is given. Fig. 9 shows the $f_0 - \theta$ relations for the $SU(3)$ value $f_8 = f_\pi$ and the ChPT estimation $f_8 = 1.25 f_\pi$. One sees that a smaller flavor singlet component of the η meson corresponds to a smaller f_0 . It

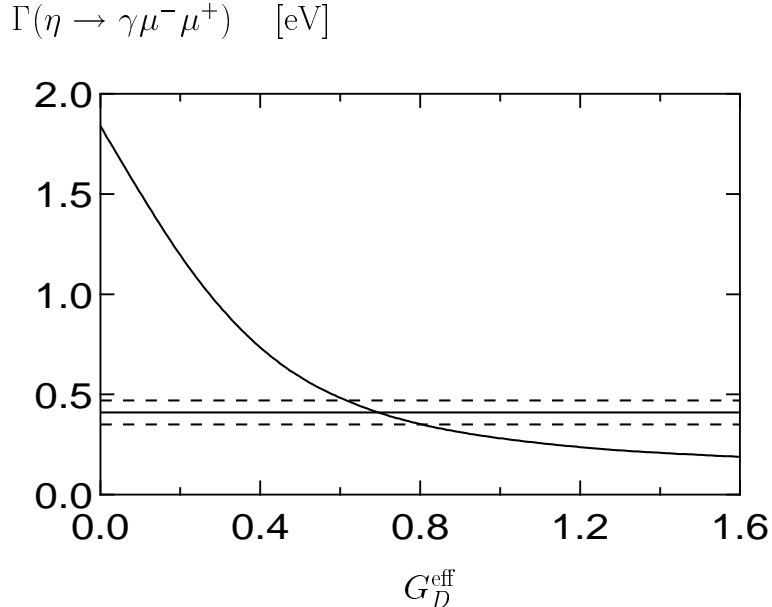


Figure 10: Dependence of the $\eta \rightarrow \gamma\mu^-\mu^+$ decay width on the dimension-less coupling constant G_D^{eff} . The horizontal solid line indicates the experimental value and the dashed lines indicate its error widths.

is not strange that f_0 is smaller than f_π since the η' meson has larger gluonic component than pion because of the $U_A(1)$ anomaly.

4.3 $\eta \rightarrow \gamma l^-l^+$ decay

The experimental value of the $\eta \rightarrow \gamma\mu^-\mu^+$ and $\eta \rightarrow \gamma e^-e^+$ decay widths are [35]⁴

$$\Gamma(\eta \rightarrow \gamma\mu^-\mu^+) = 0.41 \pm 0.06 \text{ eV}, \quad (80)$$

$$\Gamma(\eta \rightarrow \gamma e^-e^+) = 6.5 \pm 1.5 \text{ eV}, \quad (81)$$

and the calculated $\eta \rightarrow \gamma\mu^-\mu^+$ and $\eta \rightarrow \gamma e^-e^+$ decay widths are shown in Fig. 10 and Fig. 11 respectively. At $G_D^{\text{eff}} = 0.70$ where the $\eta \rightarrow \gamma\gamma$ decay width is reproduced, we obtain $\Gamma(\eta \rightarrow \gamma\mu^-\mu^+) = 0.407 \text{ eV}$, which is in good agreement with the experimental result shown in (80). On the other hand, our calculated

⁴We have used the two photon measurement result of the $\eta \rightarrow \gamma\gamma$ decay width: $\Gamma(\eta \rightarrow \gamma\gamma) = 0.510 \pm 0.026 \text{ keV}$.

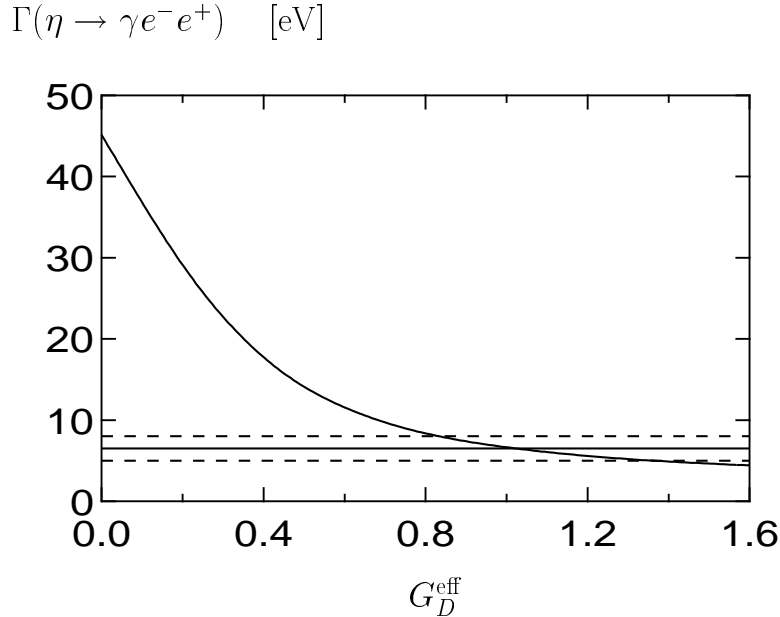


Figure 11: Dependence of the $\eta \rightarrow \gamma e^- e^+$ decay width on the dimension-less coupling constant G_D^{eff} . The horizontal solid line indicates the experimental value and the dashed lines indicate its error widths.

result of the $\eta \rightarrow \gamma e^- e^+$ at $G_D^{\text{eff}} = 0.70$ is $\Gamma(\eta \rightarrow \gamma e^- e^+) = 9.72$ eV, which is about 50% bigger than the observed value given in (81).

It is clear from the electron-positron pair invariant mass square spectrum of the $\eta \rightarrow \gamma e^- e^+$ decay given in Eq. (48) that the strength is mostly saturated in the small region just above $q^2 = (2m_e)^2$. Since in this region, the $\eta\gamma\gamma^*$ transition form factor $f_{\eta\gamma\gamma^*}(q^2)$ is almost unity and the radiative corrections are found to be negligible [37], the $\eta \rightarrow \gamma e^- e^+$ decay width is strongly related to the $\eta \rightarrow \gamma\gamma$ decay width and it is rather hard to explain the present experimental values of $\Gamma(\eta \rightarrow \gamma\gamma)$ and $\Gamma(\eta \rightarrow \gamma e^- e^+)$ simultaneously.

The calculated $\eta\gamma\gamma^*$ transition form factor $f_{\eta\gamma\gamma^*}(q^2)$ at $G_D^{\text{eff}} = 0.7$ is shown in Fig. 12 and the calculated slope parameter defined in Eq. (55) is $\Lambda_\eta = 0.94$ GeV. The recent experimental results of the slope parameter are as follows. The TPC/2γ Collaboration at the SLAC gives $\Lambda_\eta = 0.70 \pm 0.08$ GeV [38] and the CELLO Collaboration at the DESY gives $\Lambda_\eta = 0.84 \pm 0.06$ GeV [39]. So our result is somewhat larger than the experimental results. As for the slope parameter of

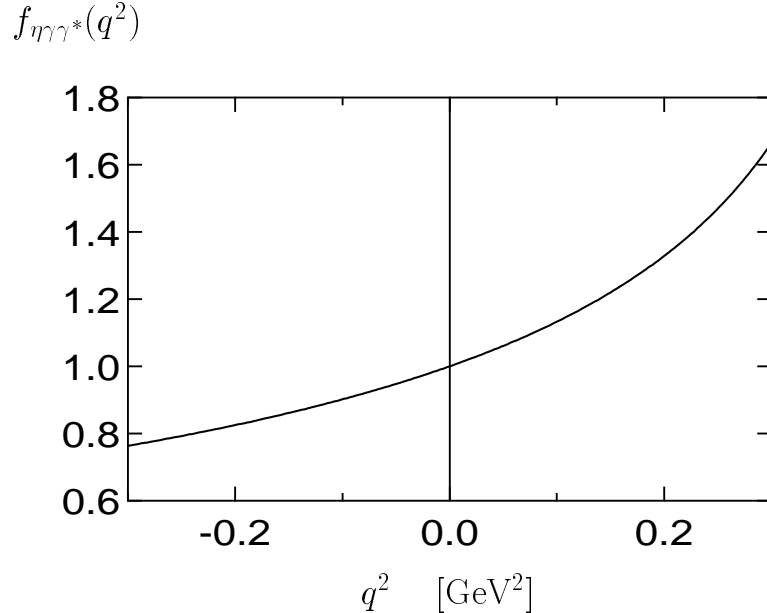


Figure 12: q^2 -dependence of the $\eta\gamma\gamma^*$ transition form factor $f_{\eta\gamma\gamma^*}(q^2)$ calculated at $G_D^{\text{eff}} = 0.7$

the $\pi^0\gamma\gamma^*$ form factor, our model gives the simple result in the chiral limit, i.e., $\Lambda_\pi = \sqrt{12}M_u \simeq 1.126$ GeV, which is also larger than the CELLO result $\Lambda_\pi = 0.75 \pm 0.03$ GeV [39].

Ametller et al. [10] studied the transition form factors for the $P\gamma\gamma^*$ vertices with $P = \pi^0$, η and η' using the most successful and/or traditional models of the low-energy QCD including the vector meson dominance model (VMD), the constituent quark loop model (QL), the QCD-inspired interpolation model by Brodsky-Lepage (BL) and the ChPT. They concluded that all the models considered agree in the correct value for a mean Λ_P , but differ in the breaking pattern of the $SU(3)$ flavor symmetry. Our approach is close to QL approach. In Ref. [10], a rather small constituent quark mass ($M_{u,d} \simeq 0.23$ GeV) has been used and that is the main reason why QL prediction of Λ_η is in reasonable agreement with the experimental results. However, it should be noted here that since the constituent quark mass used in QL is smaller than $m_\eta/2$, the unphysical imaginary part appears in the $\eta \rightarrow \gamma\gamma^*$ transition amplitude corresponding to the unphysical channel $\eta \rightarrow \bar{u}u, \bar{d}d$.

Our interpretation of the present result in the NJL model is as follows. Since the pseudoscalar mesons in the NJL model have the quark-antiquark structures and therefore have the size. For the $\pi^0\gamma\gamma^*$ vertices, it is $r_{\pi^0} \simeq 1/\sqrt{2}M_u \simeq 0.43$ fm, which is about 67% of the experimental value $r_{\pi^0} = \sqrt{6}/\Lambda_\pi \simeq 0.64$ fm. Our result of the $\eta\gamma\gamma^*$ vertex size is $r_\eta = \sqrt{6}/\Lambda_\eta \simeq 0.51$ fm, which should be compared with the experimental results $r_\eta \simeq 0.69$ fm [38] and $r_\eta \simeq 0.58$ fm [39]. The introduction of the quark-antiquark correlations in the vector channel may solve the problem of the difference of the sizes for the $P\gamma\gamma^*$ vertices between our results and the experimental ones.

4.4 $\eta \rightarrow \pi^0\gamma\gamma$ decay

The experimental value of the $\eta \rightarrow \pi^0\gamma\gamma$ decay width is [35]⁵

$$\Gamma(\eta \rightarrow \pi^0\gamma\gamma) = 0.93 \pm 0.19 \text{ eV}, \quad (82)$$

and the calculated $\eta \rightarrow \pi^0\gamma\gamma$ decay width is shown in Fig. 13. At $G_D^{\text{eff}} = 0.70$ where the $\eta \rightarrow \gamma\gamma$ decay width is reproduced, we obtain $\Gamma(\eta \rightarrow \pi^0\gamma\gamma) = 0.92 \text{ eV}$, which is in good agreement with the experimental data shown in (82).

In ChPT [11, 12], since the lowest order $O(p^2)$ term and the next order $O(p^4)$ tree diagrams do not contribute to the $\eta \rightarrow \pi^0\gamma\gamma$ process, the $O(p^4)$ one-loop diagrams are the leading contributions. The calculated pion and kaon one-loop contributions to the $\eta \rightarrow \pi^0\gamma\gamma$ decay width are $\Gamma_\pi^{(4)}(\eta \rightarrow \pi^0\gamma\gamma) = 0.84 \times 10^{-3} \text{ eV}$, $\Gamma_K^{(4)}(\eta \rightarrow \pi^0\gamma\gamma) = 2.45 \times 10^{-3} \text{ eV}$ and $\Gamma_{\pi,K}^{(4)}(\eta \rightarrow \pi^0\gamma\gamma) = 0.84 \times 10^{-3} \text{ eV}$, which are more than two orders of magnitude below the observed width (82). This is because the pion loop violates the G-parity invariance and the kaon loop is also suppressed by the large kaon mass. At $O(p^6)$, there exists contribution coming from tree diagrams, one-loops and two-loops. The loop contributions are smaller than those from the order $O(p^4)$. In [11], the coupling strengths of the $O(p^6)$ tree diagrams are determined assuming saturation by the scalar meson $a_0(980)$ and the tensor meson $a_2(1310)$ resonances as well as the ρ and ω vector meson resonances. The obtained resonance contributions are $\Gamma_{\rho+\omega}^{(6)}(\eta \rightarrow \pi^0\gamma\gamma) = 0.18 \text{ eV}$ and $\Gamma_{\rho+\omega+a_0+a_2}^{(6)}(\eta \rightarrow \pi^0\gamma\gamma) = 0.18 \pm 0.02 \text{ eV}$. The contributions of other mesons, such as $b_1(1235)$, $h_1(1170)$, $h_1(1380)$ [40] and other tree diagrams [13], are found

⁵We have used the two photon measurement result of the $\eta \rightarrow \gamma\gamma$ decay width: $\Gamma(\eta \rightarrow \gamma\gamma) = 0.510 \pm 0.026 \text{ keV}$.

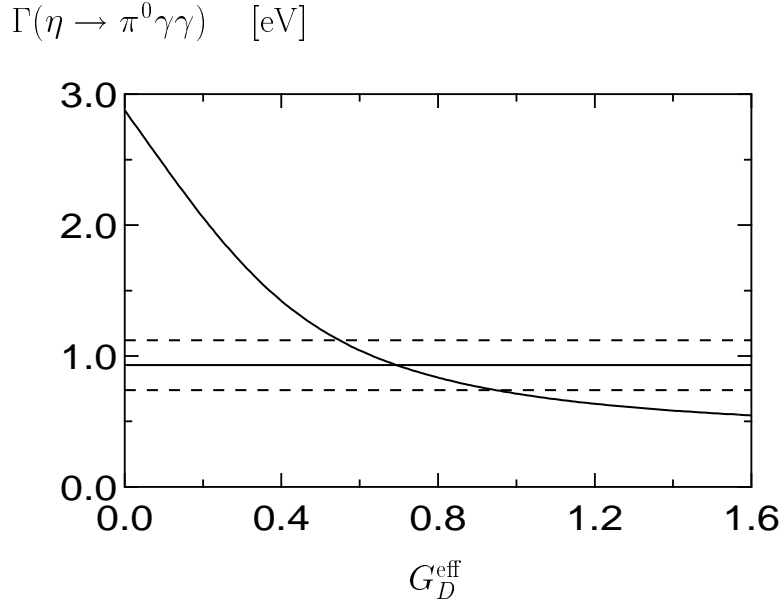


Figure 13: Dependence of the $\eta \rightarrow \pi^0\gamma\gamma$ decay width on the dimension-less coupling constant G_D^{eff} . The horizontal solid line indicates the experimental value and the dashed lines indicate its error widths.

to be small. Therefore, up to $O(p^6)$, ChPT estimation of the $\eta \rightarrow \pi^0\gamma\gamma$ decay width is about 1/4 of the experimental result.

On the other hand in [41] the $O(p^6)$ tree diagrams are evaluated by using the extended NJL (ENJL) model [42]. They calculated three contributions in ENJL, namely, the vector and scalar resonance exchange and the quark-loop contributions. Their result is $\Gamma(\eta \rightarrow \pi^0\gamma\gamma) \simeq 0.5$ eV. They further introduced the $O(p^8)$ chiral corrections as well as the axialvector and tensor meson exchange contributions, and finally obtained $\Gamma(\eta \rightarrow \pi^0\gamma\gamma) = 0.58 \pm 0.3$ eV. A recent similar analysis in ENJL concludes somewhat smaller value for the decay width [43]. The difference between our approach and that in [41] are as follows. The ENJL model lagrangian has not only the scalar-pseudoscalar four quark interactions but also the vector-axialvector four quark interactions. However, the $U_A(1)$ breaking is not explicitly included in their model and therefore the $\eta - \eta'$ mixing is introduced by hand with the mixing angle $\theta = -20^\circ$. We stress that the introduction of the $U_A(1)$ breaking interaction is important to understand the structure of the η meson. There is another difference. The coupling constants of the chiral

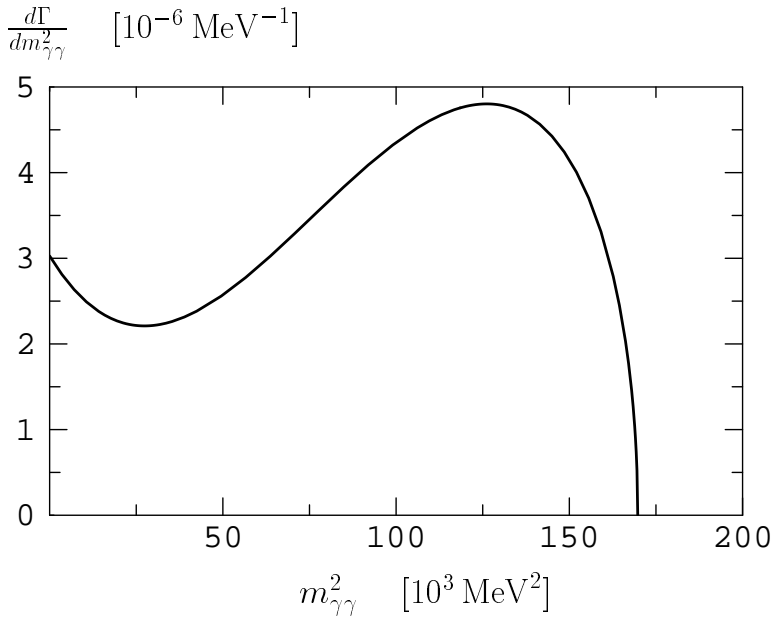


Figure 14: Spectrum of the photon invariant mass $m_{\gamma\gamma}^2$.

effective meson lagrangian predicted in the ENJL model are parameters of the Green function evaluated at zero momenta. On the other hand we evaluate the quantities at the pole position of the mesons.

Calculated spectrum of the photon invariant mass square $m_{\gamma\gamma}^2$ for the $\eta \rightarrow \pi^0\gamma\gamma$ decay is shown in Fig 14. As this spectrum is compared with those calculated by ChPT in [13], we find ours to be similar to the one for $d_3 = 4.5 \times 10^{-2}$ GeV $^{-2}$ in [13] which involves an additional $O(p^6)$ contribution to the original lagrangian. Spectrum of the photon energy E_γ for the $\eta \rightarrow \pi^0\gamma\gamma$ decay is shown in Fig 15, and given in [11] in ChPT. Both are also similar, though there is no experimental result.

In our calculation of the $\eta \rightarrow \pi^0\gamma\gamma$ decay, we evaluate only the quark-box diagram given in Fig 3. Since the vector and axialvector four-quark interactions are not included in our model, the only other contribution to this process is the scalar resonance exchange. In the ENJL model the contribution of the scalar resonance exchange is small [41]. The relevant process is $\eta \rightarrow a_0\pi^0 \rightarrow \gamma\gamma\pi^0$. Since the $a_0 \rightarrow \gamma\gamma$ decay amplitude is known to be small experimentally, the scalar resonance contribution is suppressed. Although the effect of the scalar

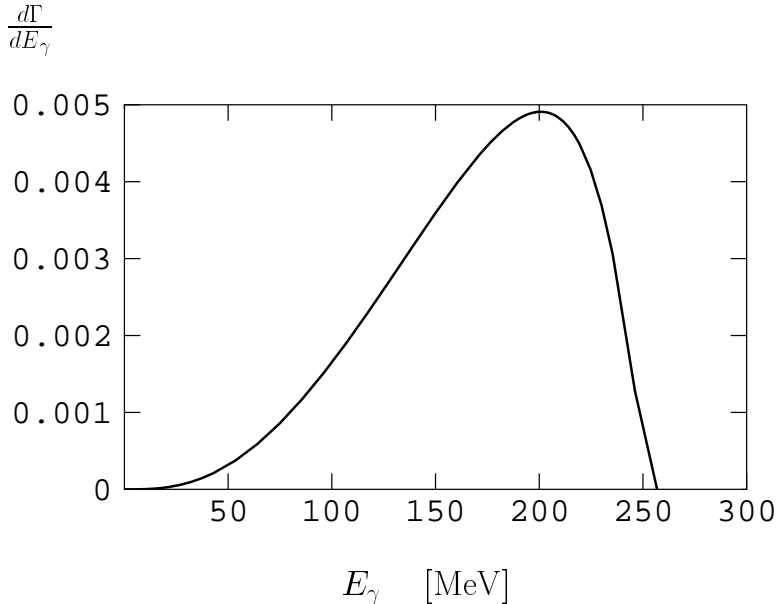


Figure 15: Spectrum of the photon energy E_γ .

channel quark-antiquark correlation is not taken into account in our calculation, the scalar resonance contribution is (partly) included in the box diagram.

If one includes the vector and axialvector four-quark interaction in the NJL model, the pseudoscalar meson properties are affected through the pseudoscalar-axialvector channel mixing and the model parameters with and without the vector and axialvector four-quark interaction are different. We expect that the models with and without the vector-axialvector interaction predict similar results for the processes involving only the pseudoscalar mesons with energies much below the vector meson masses. It is further argued that the contribution of the quark-box diagram to the $\gamma\gamma \rightarrow \pi^0\pi^0$ process, that is similar to $\eta \rightarrow \pi^0\gamma\gamma$, is quite close to that of the vector meson exchange in the vector dominance model [44].

5 Scalar Quark Contents in Nucleon

The $U_A(1)$ breaking six-quark flavor-determinant interaction \mathcal{L}_6 given in Eq. (4) gives rise to flavor mixing not only in the pseudoscalar channel but also in the scalar channel. Therefore, it is important to study the effects of the $U_A(1)$

breaking interaction in the scalar $\bar{q}q$ channels.

In the NJL model, it is known that the masses of the scalar mesons become just the twice of the constituent quark mass in the chiral limit. Introducing the explicit breaking of the chiral symmetry by the current quark masses pushes up the scalar meson masses above the quark-antiquark threshold. Since the NJL model does not confine quarks, we do not apply it to the scalar mesons in this article.

In this section we will discuss the scalar quark contents in nucleon as well as the pion-nucleon sigma term $\Sigma_{\pi N}$ and the kaon-nucleon sigma term Σ_{KN} . We use a rather naive additive quark model for the nucleon state, namely, the nucleon is made up by three noninteracting constituent quarks whose masses are determined by the gap equation shown in Eq. (5). The scalar quark content of flavor a in the proton is then obtained as follows.

$$\langle P | \bar{q}^a q^a | P \rangle = 2 \langle U | \bar{q}^a q^a | U \rangle + \langle D | \bar{q}^a q^a | D \rangle, \quad (83)$$

with $|U\rangle$ ($|D\rangle$) is the constituent u- (d-) quark state. The amount of the $\bar{q}q$ content of flavor a in a constituent quark Q of flavor b is deduced by using the Feynman-Hellman theorem, i.e.,

$$\langle Q^b | \bar{q}^a q^a | Q^b \rangle = \frac{\partial M_b}{\partial m_a}, \quad (84)$$

where m_a and M_b are the current and constituent quark masses, respectively. Here the isospin symmetry is assumed and therefore the following relations hold. $\langle U | \bar{u}u | U \rangle = \langle D | \bar{d}d | D \rangle$, $\langle U | \bar{d}d | U \rangle = \langle D | \bar{u}u | D \rangle$ and $\langle U | \bar{s}s | U \rangle = \langle D | \bar{s}s | D \rangle$.

We have calculated the scalar quark contents in the constituent u-quark as functions of G_D^{eff} and the results are shown in Fig. 16. At $G_D^{\text{eff}} = 0$, both $\langle U | \bar{d}d | U \rangle$ and $\langle U | \bar{s}s | U \rangle$ vanish as expected. Because of the larger mass of the strange quark, $\langle U | \bar{s}s | U \rangle$ is strongly suppressed compared to $\langle U | \bar{d}d | U \rangle$. At $G_D^{\text{eff}} = 0.7$, our results are

$$\langle P | \bar{u}u | P \rangle = 3.30, \quad \langle P | \bar{d}d | P \rangle = 2.10, \quad \langle P | \bar{s}s | P \rangle = 0.08, \quad (85)$$

and therefore, the strange quark content in the proton is rather small,

$$y \equiv \frac{2 \langle P | \bar{s}s | P \rangle}{\langle P | \bar{u}u + \bar{d}d | P \rangle} = 0.03. \quad (86)$$

This value is smaller than the “standard” value $y \approx 0.2$. However, as we will see later, our result depends on the choice of the current u,d-quark mass and therefore should not be taken seriously.

$$\langle U | \bar{u}u | U \rangle, \langle U | \bar{d}d | U \rangle, \langle U | \bar{s}s | U \rangle$$

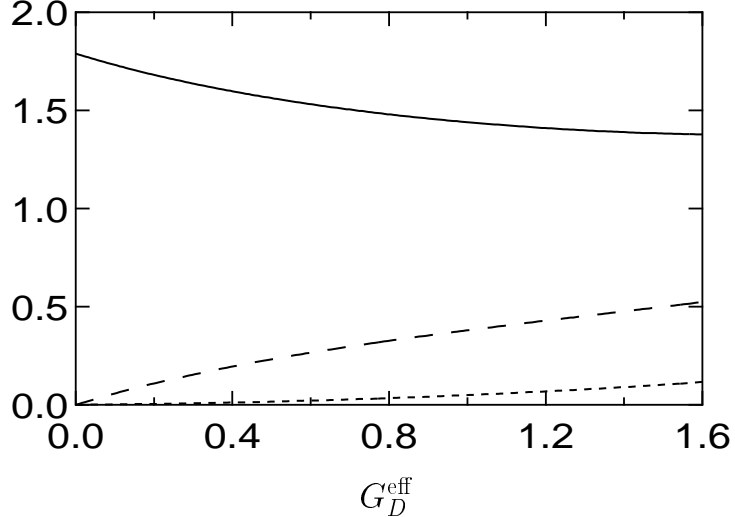


Figure 16: Dependence of the scalar quark contents in the constituent u-quark on the dimension-less coupling constant G_D^{eff} . The solid line, dashed line and dotted line indicate $\langle U | \bar{u}u | U \rangle$, $\langle U | \bar{d}d | U \rangle$ and $\langle U | \bar{s}s | U \rangle$, respectively.

Assuming the isospin symmetry, the $\Sigma_{\pi N}$ and Σ_{KN} terms are represented using the scalar quark contents in the nucleon as follows.

$$\Sigma_{\pi N} = \hat{m} \langle N | \bar{u}u + \bar{d}d | N \rangle, \quad (87)$$

$$\Sigma_{KN} = \frac{3}{2}(\hat{m} + m_s) \langle N | \frac{1}{2}(\bar{u}u + \bar{d}d) + \bar{s}s | N \rangle, \quad (88)$$

with $\hat{m} = (m_u + m_d)/2$. The calculated $\Sigma_{\pi N}$ and Σ_{KN} terms are shown in Fig. 17. The $\Sigma_{\pi N}$ term is almost independent on G_D^{eff} . At $G_D^{\text{eff}} = 0.7$, we obtained $\Sigma_{\pi N} = 43.2$ MeV which is in good agreement with the value extracted from the low-energy πN scattering data [45]: $\Sigma_{\pi N} = (45 \pm 10)$ MeV. As for the Σ_{KN} term, our result at $G_D^{\text{eff}} = 0.7$ is 280 MeV.

In the additive quark assumption of the nucleon states, the following relation holds.

$$\langle P | 2\bar{d}d - \bar{u}u | P \rangle = 3\langle U | \bar{d}d | U \rangle. \quad (89)$$

Therefore, it vanishes if there exists no flavor mixing in the scalar channel. Our result at $G_D^{\text{eff}} = 0.7$ is $\langle P | 2\bar{d}d - \bar{u}u | P \rangle = 0.89$.

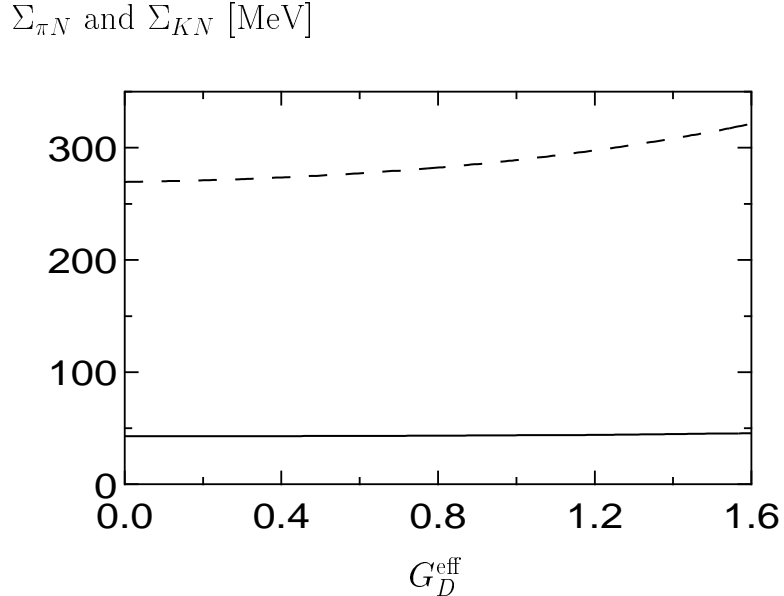


Figure 17: Dependence of the $\Sigma_{\pi N}$ and Σ_{KN} terms on the dimension-less coupling constant G_D^{eff} . The solid line indicates $\Sigma_{\pi N}$ term and the dashed line indicates Σ_{KN} terms, respectively.

The pion-nucleon sigma term and the scalar quark contents in the nucleon are extensively studied in the three-flavor NJL model in Ref. [18]. As pointed out there, the scalar quark contents in the constituent quarks depend on the current quark masses nonlinearly. In order to study this nonlinearity, we change the current u,d-quark mass from 7.5 MeV to 8.5 MeV. Other four parameters of the model (m_s , G_S , G_D and Λ) are determined so as to reproduced the observed values of m_π , m_K , m_η and f_π . Thus the size of the chiral symmetry breaking is fixed though the current u,d-quark mass is changed. The calculated results are shown in Table 1. The scalar quark contents in the constituent u-quark and the sigma terms, especially, $\langle U | \bar{s}s | U \rangle$ and Σ_{KN} depend on the current u,d-quark mass rather strongly.

We next discuss the validity of the additive quark assumption for the nucleon state. Kunihiro and Hatsuda [17, 46] studied the effects of the confinement and the short-range spin-spin interaction between the constituent quarks in baryons in the framework of the nonrelativistic potential model. They have found that the effects of the residual interactions between the constituent quarks in the

Table 1: The scalar quark contents in the constituent u-quark and the $\Sigma_{\pi N}$ and Σ_{KN} terms in the three different current u,d-quark masses.

$m_{u,d}$ [MeV]	$\langle U \bar{u}u U \rangle$	$\langle U \bar{d}d U \rangle$	$\langle U \bar{s}s U \rangle$	$\Sigma_{\pi N}$ [MeV]	Σ_{KN} [MeV]
7.5	1.582	0.707	0.210	51.5	390.6
8.0	1.388	0.478	0.091	44.8	308.8
8.5	1.232	0.300	0.009	39.1	243.0

proton increase the $\bar{u}u$, $\bar{d}d$ and $\bar{s}s$ contents of the proton by about 5%, 24% and 13%, respectively. The contributions of the kinetic term of the confined quark are flavor independent and negative, while those of the short-range spin-spin interaction are flavor dependent and positive. The flavor-mixing effect by the short-range spin-spin interaction is rather large. For simplicity, we consider the $\langle U | \bar{d}d | U \rangle = \langle U | \bar{s}s | U \rangle = 0$ case. Using the expression of $\langle P | \bar{q}_i q_i | P \rangle$ given in Ref. [17], one obtains

$$\langle P | 2\bar{d}d - \bar{u}u | P \rangle = \frac{6b}{M_u^3} \langle U | \bar{u}u | U \rangle, \quad (90)$$

where $b = (176.4 \text{ MeV})^3$ is the strength of the short-range spin-spin interaction. Inserting our numerical results at $G_D^{\text{eff}} = 0$, i.e., $M_u = 325 \text{ MeV}$ and $\langle U | \bar{u}u | U \rangle = 1.79$, we get $\langle P | 2\bar{d}d - \bar{u}u | P \rangle = 1.72$.

Recently, the static properties of the nucleon have been studied in the relativistic Faddeev approach using the two-flavor NJL model [47]. Their results of the scalar quark contents in the nucleon are $\langle P | \bar{u}u | P \rangle = 1.795$ and $\langle P | \bar{d}d | P \rangle = 1.095$. Since the single quark renormalization factor $\partial M / \partial m$ is not included in their calculations, one should compare above numbers with those in the additive quark model, i.e., $\langle P | \bar{u}u | P \rangle = 2$ and $\langle P | \bar{d}d | P \rangle = 1$. The residual interactions between quarks in the nucleon decrease the u-quark content by about 10% and increase the d-quark content by about 10%. It is a contrast to the results in the nonrelativistic quark model. As for the flavor mixing effect, one gets $\langle P | 2\bar{d}d - \bar{u}u | P \rangle = 0.395 \langle U | \bar{u}u | U \rangle \simeq 0.71$. Here we have used our result: $\langle U | \bar{u}u | U \rangle = 1.79$. In the nonrelativistic quark model approach, the flavor mixing effect entirely comes from the short-range spin-spin interaction. On the other hand, in the relativistic Faddeev approach, only the scalar diquark state is included. Inclusion of the axialvector diquark may be important for the flavor

mixing in the scalar quark contents in the nucleon.

In the above two approaches, the effects of the pion cloud around the quark-core of the nucleon is not taken into account. Wakamatsu has studied the scalar quark contents in the nucleon using the chiral quark soliton model as functions of the constituent u,d-quark mass [48]. His results are as follows. At $M_{u,d} = 350\text{MeV}$, $\langle P | \bar{u}u | P \rangle = 1.807$, $\langle P | \bar{d}d | P \rangle = 1.223$ and at $M_{u,d} = 450\text{MeV}$, $\langle P | \bar{u}u | P \rangle = 1.382$, $\langle P | \bar{d}d | P \rangle = 0.978$. As discussed in [48], the flavor-asymmetry of the sea-quark in the nucleon gives rise to the flavor mixing phenomena and the calculated results are $\langle P | 2\bar{d}d - \bar{u}u | P \rangle = 0.639$ at $M_{u,d} = 350\text{MeV}$ and $\langle P | 2\bar{d}d - \bar{u}u | P \rangle = 0.574$ at $M_{u,d} = 450\text{MeV}$. Since the chiral quark soliton model do not have the dynamics of the spontaneous breaking of chiral symmetry, the effects of the single quark renormalization factor $\partial M / \partial m$ is not taken into account.

In conclusion, as is expected, the flavor mixings in the scalar channel are approximately proportional to the strength of the $U_A(1)$ breaking interaction in the NJL model. However their magnitudes depend on the choice of the model parameters. Furthermore, the scalar quark contents in the proton have many origins, and therefore we cannot draw a definite conclusion on the effects of the $U_A(1)$ breaking interaction.

6 Effects of the $U_A(1)$ Anomaly in Baryons

Since the effects of the $U_A(1)$ anomaly are rather large in the pseudoscalar sector, it is natural to ask if one can see some effects in the baryon sector. It was pointed out in [24] that the instanton can play an important role in the description of spin-spin forces, particularly for light baryons. The pattern of these effects can be very hard to disentangle from one-gluon exchange. The effects of the instanton induced interaction in baryon number $B = 2$ systems were studied in [25]. It was shown that an attraction between two nucleons is obtained by the two-body instanton induced interaction, while the three-body interaction is strongly repulsive in the H-dibaryon channel and makes the H-dibaryon almost unbound.

We estimate the effects of the $U_A(1)$ anomaly on the $B = 1$ and $B = 2$ systems by employing the six-quark determinant interaction given in Eq. (4) whose strength was determined so as to reproduce the observed η -meson mass,

Table 2: Contribution of the two-body term to octet and decuplet baryons. All the entries are in units of MeV.

wave function	N	Σ	Ξ	Λ	Δ	Σ^*	Ξ^*	Ω
MIT	-43.9	-41.2	-41.2	-42.9	0	0.12	0.12	0
NRQM	-40.88	-36.6	-36.6	-39.4	0	0.07	0.07	0

Table 3: Baryon component, $SU(3)$ multiplet, spin, isospin and strangeness of the eight channels of two octet baryons.

channel	Baryon component	$SU(3)$ multiplet	Spin	Isospin	Strangeness
I	NN	10*	1	0	0
II	NN	27	0	1	0
III	$N\Sigma$	27	0	3/2	-1
IV	$N\Sigma - N\Lambda$	27	0	1/2	-1
V	$N\Sigma - N\Lambda$	10*	1	1/2	-1
VI	$N\Sigma$	10	1	3/2	-1
VII	$N\Sigma - N\Lambda$	8	1	1/2	-1
VIII	H	1	0	0	-2

the $\eta \rightarrow \gamma\gamma$ decay width and the $\eta \rightarrow \pi^0\gamma\gamma$ decay width, namely, $G_D^{\text{eff}} = 0.7$. It is done by calculating the matrix elements of the the $U_A(1)$ breaking interaction hamiltonian with respect to unperturbed states of the MIT bag model and the nonrelativistic quark model (NRQM). For $B = 2$ systems, we only consider the $(0S)^6$ configuration of the six valence quark states. Therefore, the matrix element with respect to such a state gives a measure of the contribution of the $U_A(1)$ breaking interaction either to the dibaryon or to the short-range part of the interaction between two baryons. The determinant interaction induces not only three-body but also two-body interactions of valence quarks when the vacuum has a nonvanishing quark condensate. The details of the calculation are described in [26].

Table 2 shows the contribution of the two-body term for $B = 1$. The contribution to the decuplet baryons vanishes in the $SU(3)$ limit and therefore comes only from the $SU(3)$ asymmetry of the quark wave function. The three-body term does not contribute to the $B = 1$ states. Thus the $N\Delta$ mass difference due

Table 4: Contributions of the two-body term to the eight channels of two octet baryons listed in Table 3. All the entries are in units of MeV.

wave function	I	II	III	IV	V	VI	VII	VIII
MIT	-90	-85	-89	-86	-94	-97	-122	-163
NRQM	-120	-105	-102	-104	-118	-117	-148	-183

Table 5: Contributions of the three-body term to the H-dibaryon (VIII) and strangeness -1 two octet baryon channels (III-VII). All the entries are in units of MeV.

wave function	III	IV	V	VI	VII	VIII
MIT	-6×10^{-2}	-6×10^{-2}	-7×10^{-2}	20.7	25.1	40.7
NRQM	-5×10^{-2}	-5×10^{-2}	-5×10^{-2}	28.3	34.9	56.1

to the $U_A(1)$ breaking interaction is about 15% of the observed one.

We next discuss the case of $B = 2$. We consider all the possible channels which are made of two octet baryons listed in Table 3. Table 4 shows the contribution of the two-body term. The channel VIII gets the strongest attraction, about 170 MeV, and the channel VII gets the second strongest attraction. The contributions of the three-body term to the H-dibaryon and strangeness -1 channels are given in Table 5. It should be noted that the three-body term has no effect on the NN channels, and that the contributions to the channels III, IV and V reflect the $SU(3)$ breaking in the quark wave function. The contributions of the three-body term in channels VI, VII and VIII are remarkable and one will be able to observe some effects experimentally.

We should comment on the difference between the determinant interaction used here and the instanton-induced interaction used in ref. [25]. The relative contributions of the $U_A(1)$ breaking interaction within the baryonic sector or within the mesonic sector are similar for the two interactions. However, the ratio of those in the baryonic sector to those in the mesonic sector is about $\frac{4}{7}$. Namely, if one fixes the strength of the interaction so as to give the same mass difference of η and η' , the effects of the instanton-induced interaction in the baryonic sector would be about $\frac{7}{4}$ stronger than those of the determinant interaction. After this

correction the strength of the present $U_A(1)$ breaking interaction is consistent with that used in the calculation of the baryon-baryon interaction in ref. [25].

7 Summary and conclusions

Using an extended three-flavor NJL model that includes the 't Hooft instanton induced $U_A(1)$ breaking interaction, we have studied the $\eta \rightarrow \gamma\gamma$, $\eta \rightarrow \gamma\mu^-\mu^+$, $\eta \rightarrow \gamma e^-e^+$, and $\eta \rightarrow \pi^0\gamma\gamma$ decays as well as the η -meson mass, η decay constant and flavor $SU(3)$ singlet-octet mixing angle θ of the η meson. Advantages of our approach are as follows. (1) Effects of the explicit chiral symmetry breaking by the current quark masses and the $U_A(1)$ anomaly can be evaluated consistently on the η -meson decay amplitudes. (2) One can study how the η -meson properties change when the strength of the $U_A(1)$ breaking interaction is changed.

We have found that the η -meson mass, the $\eta \rightarrow \gamma\gamma$, $\eta \rightarrow \gamma\mu^-\mu^+$ and $\eta \rightarrow \pi^0\gamma\gamma$ decay widths are in good agreement with the experimental values when the $U_A(1)$ breaking is strong and the mixing angle θ is about zero.

The calculated η decay constant is almost independent of the strength of the $U_A(1)$ breaking interaction and is close to the pion decay constant. It indicates that the η meson does not lose the the Nambu-Goldstone boson nature though its mass and mixing angle are strongly affected by the $U_A(1)$ breaking interaction.

Our result of the mixing angle θ is about zero which is different from the value $\theta \simeq -20^\circ$ obtained in the PCAC + ABJ anomaly approach and ChPT. We have discussed the possible origin of this difference in Sect. 4.2. It should be stressed here that the $\eta' \rightarrow \gamma\gamma$ decay width is used to obtain the mixing angle in the PCAC and ChPT approaches. However, since the η' meson is heavy, it is rather questionable to study the $\eta' \rightarrow \gamma\gamma$ decay in the PCAC and ChPT approaches.

Since the 't Hooft instanton induced $U_A(1)$ breaking interaction gives rise to the flavor mixing not only in the pseudoscalar $\bar{q}q$ channels but also in the scalar $\bar{q}q$ channels, we have studied the scalar quark contents in the nucleon, the pion-nucleon and the kaon-nucleon sigma terms. The calculated pion-nucleon sigma term is almost independent of the strength of the $U_A(1)$ breaking interaction and in good agreement with the value extracted from the low-energy πN scattering data. Concerning the flavor mixing effects, we have found that the amount of the flavor mixing in the scalar quark contents in the nucleon depends on the strength of the spontaneous breaking of chiral symmetry and the residual interactions

between the constituent quarks in the nucleon rather strongly. In this sense, the scalar quark contents of the nucleon are interesting and important quantities. Further studies are necessary.

We have estimated the effects of the $U_A(1)$ anomaly on the baryon number $B = 1$ and $B = 2$ systems too. We have found that the $N\Delta$ mass difference due to the $U_A(1)$ breaking interaction is about 15% of the observed one and the three-body term of the $U_A(1)$ breaking interaction gives 40-50 MeV repulsion in the H-dibaryon channel.

Finally, we should note that the NJL model does not confine quarks. Since the Nambu-Goldstone bosons, π , K and η are strongly bound, the NJL can describe their properties fairly well. However the η' -meson state in the NJL model has an unphysical decay of $\eta' \rightarrow q\bar{q}$. Therefore, we do not apply our model to the η' meson. In order to study the role of the $U_A(1)$ anomaly on the low-energy QCD further, the studies of the η' -meson properties are desirable.

References

- [1] G. 't Hooft, Nucl. Phys. B **72** (1974) 461;
For a review; G.A. Christos, Phys. Rep. **116** (1984) 251.
- [2] G. Veneziano, Nucl. Phys. B **159** (1979) 213.
- [3] S. Adler, Phys. Rev. **177** (1969) 2426;
J. Bell and R. Jackiw, Nuovo Cimento **60A** (1969) 47.
- [4] J. Wess and B. Zumino, Phys. Lett. B **37** (1971) 95.
- [5] E. Witten, Nucl. Phys. B **223** (1983) 422.
- [6] J.F. Donoghue, B.R. Holstein and Y.-C.R. Lin, Phys. Rev. Lett. **55** (1985) 2766; **61** (1988) 1527 (E);
J. Bijnens, A. Bramon and F. Cornet, Phys. Rev. Lett. **61** (1988) 1453;
J.F. Donoghue and D. Wyler, Nucl. Phys. B **316** (1989) 289.
- [7] J. Gasser and H. Leutwyler, Ann. of Phys. **158** (1984) 142.
- [8] J. Gasser and H. Leutwyler, Nucl. Phys. B **250** (1985) 465.
- [9] G.M. Shore and G. Veneziano, Nucl. Phys. B **381** (1992) 3.
- [10] Ll. Ametller, J. Bijnens, A. Bramon and F. Cornet, Phys. Rev. D **45** (1992) 986.
- [11] Ll. Ametller, J. Bijnens, A. Bramon and F. Cornet, Phys. Lett. B **276** (1992) 185.
- [12] M. Jetter, Nucl. Phys. B **459** (1996) 283.
- [13] P. Ko, Phys. Lett. B **349** (1995) 555.
- [14] G. 't Hooft, Phys. Rev. D **14** (1976) 3432.
- [15] M. Kobayashi, H. Kondo and T. Maskawa, Prog. Theor. Phys. **45** (1971) 1955.
- [16] T. Kunihiro and T. Hatsuda, Phys. Lett. B **206** (1988) 385;
T. Hatsuda and T. Kunihiro, Z. Phys. C **51** (1991) 49.

- [17] T. Hatsuda and T. Kunihiro, *Phys. Rep.* **247** (1994) 221.
- [18] V. Bernard, R.L. Jaffe and U.-G. Meissner, *Nucl. Phys. B* **308** (1988) 753.
- [19] Y. Kohyama, K. Kubodera and M. Takizawa, *Phys. Lett. B* **208** (1988) 165; M. Takizawa, K. Tsushima, Y. Kohyama and K. Kubodera, *Prog. Theor. Phys.* **82** (1989) 481; *Nucl. Phys. A* **507** (1990) 611.
- [20] H. Reinhardt and R. Alkofer, *Phys. Lett. B* **207** (1988) 482; R. Alkofer and H. Reinhardt, *Z. Phys. C* **45** (1989) 275.
- [21] S. Klimt, M. Lutz, U. Vogl and W. Weise, *Nucl. Phys. A* **516** (1990) 429; U. Vogl, M. Lutz, S. Klimt and W. Weise, *Prog. Part. Nucl. Phys.* **27** (1991) 195.
- [22] M. Takizawa and M. Oka, *Phys. Lett. B* **359** (1995) 210; **364** (1995) 249 (E).
- [23] Y. Nemoto, M. Oka and M. Takizawa, hep-ph/9602253, to be published in *Phys. Rev. D*.
- [24] E.V. Shuryak and J.L. Rosner, *Phys. Lett. B* **218** (1989) 72.
- [25] M. Oka and S. Takeuchi, *Phys. Rev. Lett.* **63** (1989) 1780; *Nucl. Phys. A* **524** (1991) 649; S. Takeuchi and M. Oka, *Phys. Rev. Lett.* **66** (1991) 1271.
- [26] O. Morimatsu and M. Takizawa, *Nucl. Phys. A* **554** (1993) 635.
- [27] F.J. Gilman and R. Kauffman, *Phys. Rev. D* **36** (1987) 2761.
- [28] C. Itzykson and J.-B. Zuber, *Quantum field theory*, (McGraw-Hill, 1980) p. 550.
- [29] D. Ebert and H. Reinhardt, *Nucl. Phys. B* **271** (1986) 188.
- [30] M. Wakamatsu, *Ann. of Phys.* **193** (1989) 287.
- [31] V. Bernard and U.-G. Meissner, *Phys. Rev. Lett.* **61** (1988) 2296.
- [32] J.N. Ng and D.J. Peters, *Phys. Rev. D* **47** (1993) 4939.
- [33] G. Ecker, A. Pich and E. de Rafael, *Nucl. Phys. B* **303** (1988) 665.

- [34] H. Leutwyler, Phys. Lett. B **378** (1996) 313.
- [35] Particle Data Group, Phys. Rev. D **50** (1994) 1173.
- [36] V. Bernard, A.H. Blin, B. Hiller, U.-G. Meissner and M.C. Ruivo, Phys. Lett. B **305** (1993) 163.
- [37] B.E. Lautrup and J. Smith, Phys. Rev. D **3** (1971) 1122.
- [38] TPC/2 γ Collaboration, H. Aihara et al., Phys. Rev. Lett. **64** (1990) 172.
- [39] CELLO Collaboration, H.-J. Behrend et al., Z. Phys. C **49** (1991) 401.
- [40] P. Ko, Phys. Rev. D **47** (1993) 3933.
- [41] S. Bellucci and C. Bruno, Nucl. Phys. B **452** (1995) 626.
- [42] J. Bijnens, C. Bruno and E. de Rafael, Nucl. Phys. B **390** (1993) 501.
- [43] J. Bijnens, A. Fayyazuddin and J. Prades, Phys. Lett. B **379** (1996) 209.
- [44] J. Bijnens, S. Dawson and G. Valencia, Phys. Rev. D **44** (1991) 3555.
- [45] J. Gasser, H. Leutwyler and M. Sainio, Phys. Lett. B **253** (1991) 252.
- [46] T. Kunihiro and T. Hatsuda, Phys. Lett. B **240** (1990) 209.
- [47] H. Asami, N. Ishii, W. Bentz and K. Yazaki, Phys. Rev. C **51** (1995) 3388.
- [48] M. Wakamatsu, Phys. Rev. D **46** (1992) 3762.